BJ www.biochemj.org

BJ Structure

Biochem. J. (2011) **439**, 235–248 (Printed in Great Britain) doi:10.1042/BJ20110890

online data

Characterization of the dehydratase WcbK and the reductase WcaG involved in GDP-6-deoxy-*manno*-heptose biosynthesis in *Campylobacter jejuni*

Matthew McCALLUM*, Gary S. SHAW† and Carole CREUZENET*[1]

*Department of Microbiology and Immunology, Infectious Diseases Research Group, University of Western Ontario, London, ON, Canada, N6A 5C1, and †Department of Biochemistry, University of Western Ontario, London, ON, Canada, N6A 5C1

The capsule of *Campylobacter jejuni* strain 81-176 comprises the unusual 6-deoxy-α-D-*altro*-heptose, whose biosynthesis and function are not known. In the present study, we characterized enzymes of the capsular cluster, WcbK and WcaG, to determine their role in 6-deoxy-*altro*-heptose synthesis. These enzymes are similar to the *Yersinia pseudotuberculosis* GDP-*manno*-heptose dehydratase/reductase DmhA/DmhB that we characterized previously. Capillary electrophoresis and MS analyses showed that WcbK is a GDP-*manno*-heptose dehydratase whose product can be reduced by WcaG, and that WcbK/WcaG can use the substrate GDP-mannose, although with lower efficiency than heptose. Comparison of kinetic parameters for WcbK and DmhA indicated that the relaxed substrate specificity of WcbK comes at the expense of catalytic performance on GDP-*manno*-heptose. Moreover, although WcbK/WcaG and DmhA/DmhB are involved in *altro*- versus *manno*-heptose synthesis respectively, the enzymes can be used interchangeably in mixed reactions. NMR spectroscopy analyses indicated conservation of the sugar *manno* configuration during catalysis by WcbK/WcaG. Therefore additional capsular enzymes may perform the C3 epimerization necessary to generate 6-deoxy-*altro*-heptose. Finally, a conserved residue (Thr^{187} in WcbK) potentially involved in substrate specificity was identified by structural modelling of mannose and heptose dehydratases. Site-directed mutagenesis and kinetic analyses demonstrated its importance for enzymatic activity on heptose and mannose substrates.

Key words: *Campylobacter jejuni*, capsule synthesis, C6 dehydratase, C4 reductase, GDP-6-deoxy-*altro*-heptose, heptose modification.

INTRODUCTION

Campylobacter jejuni is a bacterial pathogen that causes endemic and traveller's gastroenteritis, reactive arthritis, neurological disorders and intestinal adenomas [1–3]. In developed countries, *C. jejuni* infections are usually associated with consumption of contaminated food. Being a commensal in birds, *C. jejuni* is naturally present in poultry faecal matter, and contamination of poultry meat by *C. jejuni* occurs very readily during slaughter of the birds and downstream processing. Incidence rates of contamination of retail poultry products by *C. jejuni* are alarming in most developed countries [4,5]. As a result, food-borne campylobacteriosis associated with consumption of undercooked poultry is a common problem [6]. For example, this pathogen causes yearly >10000 cases of campylobacteriosis in Canada, which is more than pathogenic *Escherichia coli* and *Salmonella* infections combined [7]. *C. jejuni* is also the cause of considerable morbidity and mortality for the very young and the elderly in developing countries, where infection is mostly contracted via consumption of improperly sanitized water often initially contaminated by bird droppings. Although efficient antibiotics against *C. jejuni* exist, antibiotic-resistant strains are a serious concern [7–9]. Hence novel treatment avenues are needed to treat infected patients or to eradicate *C. jejuni* from chicken before slaughter. This requires identifying novel anti-campylobacter targets.

C. jejuni produces a capsule that is important for its virulence [10–12]. The capsule comprises modified heptoses that are present as 6-deoxy or 6-*O*-methyl derivatives with various sugar ring configurations (L-*gluco*-, D-*altro*-, *ido*- heptose) depending on the strain [13–16]. These heptose derivatives may be present as a side branch or may be part of the main capsular chain. The contribution of the modified heptoses to capsular function and bacterial virulence is not known. Likewise, *Burkholderia pseudomallei* harbours 6-deoxy-L-*talo* heptose in its capsule and the capsule is important for virulence [17,18], but the precise role played by the modified heptose in capsular function is unknown. However, in *Yersinia pseudotuberculosis*, we demonstrated previously that the 6-deoxy-D-*manno*-heptose that is present in the lipopolysaccharide [19–21] affects the barrier function of the lipopolysaccharide and affects the overall virulence of *Y. pseudotuberculosis* [22]. Because the modified heptoses are not found in mammals, inhibiting bacterial heptose-modifying enzymes should not affect host metabolism. Therefore the enzymes responsible for the synthesis of modified heptoses could serve for the development of inhibitors against *Campylobacter* and other bacterial pathogens that produce heptose derivatives. These enzymes may also be interesting as glyco-engineering tools, allowing the synthesis of carbohydrate epitopes containing modified heptoses that would be useful for vaccination against pathogenic bacteria. This requires a better understanding of the biosynthesis of the modified heptoses, including the molecular basis for the enzymes' substrate and product specificities. The presence of 6-deoxy-heptoses of various sugar configurations in the surface carbohydrates of various bacterial species offers a golden opportunity to address this question.

Our laboratory has characterized the biosynthesis pathway for 6-deoxy-D-*manno*-heptose of *Y. pseudotuberculosis* at the biochemical and genetic levels. In this bacterium, the C6 GDP-*manno*-heptose dehydratase DmhA and the associated

Abbreviations used: CE, capillary electrophoresis; CV, column volume(s); DSS, 2,2-dimethylsilapentane-5-sulfonic acid; GMD, GDP-D-mannose 4,6-dehydratase; HSQC, heteronuclear single-quantum coherence; MALDI, matrix-assisted laser-desorption ionization; MS/MS, tandem MS; TEAB, triethylammonium bicarbonate.

[1] To whom correspondence should be addressed (email ccreuzen@uwo.ca).

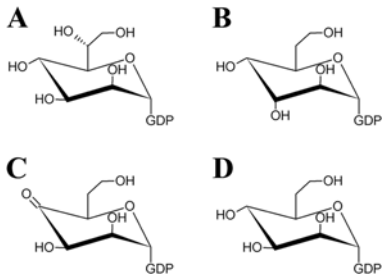

Figure 1 Schematic representation of the sugar nucleotides in the present study

(**A**) GDP-D-*manno*-heptose. (**B**) GDP-6-deoxy-D-*altro*-heptose. (**C**) GDP-4-oxo,6-deoxy-D-*lyxo*-heptose. (**D**) GDP-6-deoxy-D-*manno*-heptose.

C4 reductase DmhB are responsible for the formation of the GDP-6-deoxy-*manno*-heptose that is ultimately used for lipopolysaccharide synthesis [22–24]. A DmhA homologue, WcbK, is encoded by the capsule gene cluster of *C. jejuni* strain 81-176, which harbours 6-deoxy-α-D-*altro*-heptose in its capsule [13,25]. WcbK is 78 % identical with and 87 % similar to DmhA. A DmhB homologue, WcaG (also formerly known as HrEpiD), is also encoded by the capsule gene cluster of this *C. jejuni* strain, but only exhibits 23 % identity and 43 % similarity with DmhB. The fact that the heptose found in the capsule of *C. jejuni* strain 81-176 is in the D-*altro* configuration indicates that a C3 epimerization step occurs along the biosynthetic pathway to alter the heptose ring from the D-*manno* configuration found in the precursor to the D-*altro* found in the capsule (Figures 1A and 1B). It is not known whether WcbK, WcaG or an independent C3 epimerase will carry out this modification.

We undertook the biochemical characterization of WcbK and WcaG to establish their role in 6-deoxy-*altro* heptose formation and to determine whether they present novel substrate and product specificities compared with their DmhA/DmhB counterparts. Using a combination of CE (capillary electrophoresis), MS and NMR spectroscopy analyses, we investigated whether WcbK could use GDP-D-*manno*-heptose or GDP-mannose as a substrate, whether its reaction products were the same as the products obtained with DmhA and compared its catalytic efficiency with DmhA. We also investigated whether WcaG could serve as an acceptor for the WcbK and DmhA reaction products, and compared the reaction products generated by WcaG with those generated by DmhB. NMR spectroscopy analyses were performed to determine whether WcbK or WcaG had any epimerization activity. Finally, structural modelling and site-directed mutagenesis identified an important residue for substrate binding and/or catalysis in WcbK.

EXPERIMENTAL

Cloning of *wcbK and wcaG* in the pET vector

The *wcbK* and *wcaG* genes from *C. jejuni* 81-176 (kindly provided by Dr P. Guerry, Enteric Diseases Program, Naval Medical Research Center, Silver Spring, MD, U.S.A.) were PCR-amplified from chromosomal DNA using the primers WcbKP2/P3 and WcaGP2/P3 (Table 1) and using Pfu DNA polymerase as recommended by the manufacturer (Stratagene). The PCR products were digested with NcoI and BamHI, and were cloned into the pET23 derivative [26] with an N-terminal His tag. The constructs were used for transformation into *E. coli* DH5α with ampicillin selection (100 μg/ml). The resulting plasmids pET-*wcbK* and pET-*wcaG* were then purified using the GFX kit (GE Healthcare) and verified by DNA sequencing. The sequencing was performed at the Robarts Institute Sequencing Facility (London, ON, Canada).

Table 1 Primers used for cloning and site-directed mutagenesis

The NcoI and BamHI sites used for cloning in the pET system are highlighted in bold. The mutated codons used in site-directed mutagenesis of Thr^{187} in WcbK are underlined.

Primer name	Sequence (5′→3′)
WcaGP2	AGGTT**CCATGG**GCATGTTAAAAAAAGTTTTAATTACAGGC
WcaGP3	CT**GGATCC**GGTACCTTAAACATTTGCAAAGCGATTAACT
WbcKP2	AGGTT**CCATGG**GCATGAAAAAAACAGCGTTAATTACAG
WbcKP3	CA**GGATCC**GGTACCATTATCGATTTAAAGGAATTCTGCC
WcbKP4	CACTTTTGTTACAAGAATGGGAAATCATAGTGGCCCAAGGCGTTCTG
WcbKP5	CAGAACGCCTTGGGCCACTATGATTTCCCATTCTTGTAACAAAAGTG
WcbKP6	CTTTTGTTACAAGAATGGGAGTACATAGTGGCCCAAGGCG
WcbKP7	CGCCTTGGGCCACTATGTACTCCCATTCTTGTAACAAAAG

Site-directed mutagenesis

Site-directed mutagenesis was performed according to the QuikChange® mutagenesis procedure using Pfu Turbo DNA polymerase to construct the T187N and T187V mutants of WcbK. The primers used were WcbKP4 and P5 for T187N, and WcbKP6 and P7 for T187V (Table 1). For each mutant, two independent 25 μl reactions comprising one primer each (10 pmol), 20 ng of pET-*wcbK* template plasmid and 0.62 units of Pfu enzyme in 1 × Pfu buffer were set up. The PCR programme comprised a 2 min denaturation at 95 °C, followed by cycles of 30 s at 95 °C, 1 min at 55 °C and 6 min at 72 °C. After ten PCR cycles, 12.5 μl of each individual reaction were combined, 0.62 units of Pfu enzyme were added, and PCR was resumed for 20 more cycles as described previously [27]. The PCR products were digested with DpnI (Stratagene) and were used to transform *E. coli* DH5α with selection on 100 μg/ml ampicillin. The plasmids extracted from independent clones were sequenced using the T7 promoter primer and WcbKP3 (Table 1) to check for the exclusive presence of the desired mutations.

Protein expression and purification

Protein expression for WcaG and WcbK (wild-type and mutants) was performed in *E. coli* BL21(DE3)pLys, using LB (Luria–Bertani) broth supplemented with 100 μg/ml ampicillin and 34 μg/ml chloramphenicol. Protein expression was induced by the addition of 0.15 mM isopropyl β-D-thiogalactopyranoside. Induction was carried out at room temperature (22 °C) for 3 h. For DmhA and DmhB, overexpression of the proteins was performed as described previously [23]. For all proteins, the cells were harvested by centrifugation (15 300 ***g***, 20 min) at the end of the induction period and stored at − 20 °C until needed.

Protein expression was checked by SDS/PAGE analysis (10 % gel) with Coomassie Blue staining or anti-His tag Western blotting using a mouse anti-His IgG antibody (Sigma–Aldrich) and an Alexa Fluor® 680-labelled goat anti-mouse IgG antibody (Molecular Probes). Detection was performed using a LI-COR Odyssey Infrared Imaging System.

Purification of His-tagged WcbK and WcaG by nickel chelation

The induced cell pellets were resuspended in 30 ml of binding buffer (20 mM imidazole, 20 mM Tris/HCl and 0.5 M NaCl) adjusted to pH 8.0 for WcbK and pH 7.0 for WcaG. Lysozyme was added (150 μg/ml) and the sample was incubated on ice for 15 min

before being passed through a French press three times. Cellular debris and insoluble proteins were removed by centrifugation for 20 min at 15300 ***g***. The samples were then subjected to ultracentrifugation at 40000 rev./min for 45 min using a Ti 70 rotor. The proteins were purified by FPLC using a 1.6 ml Poros MC 20 column (4.6 mm × 100 mm; Applied Biosystems) that had been loaded with nickel sulfate and equilibrated with 10 CV (column volumes) of binding buffer. The sample was passed through the column twice before the column was washed with 10 CV of binding buffer. The proteins of interest were eluted by a linear gradient of imidazole from a concentration of 50 mM to 1 M in 30 CV. The fractions that contained the pure protein of interest were pooled and dialysed (cut-off of 3500 Da) in 50 mM Tris/HCl, pH 8.0, overnight at 4 °C. The purified proteins were analysed by SDS/PAGE as described above and were stored in 50 % glycerol at − 20 °C.

Cross-linking experiments

Cross-linking was performed using 0.25 % glutaraldehyde in water and 12–30 μg of enzymes. The reactions were incubated for 1 h at room temperature and the samples were boiled and analysed by SDS/PAGE with Coomassie Blue staining.

Preparation of GDP-*manno*-heptose substrate

GDP-*manno*-heptose substrate was prepared enzymatically from sedoheptulose 7-phosphate (GlycOTeam) using overexpressed and purified GmhA/B/C and D enzymes from *Aneurinibacillus thermoaerophilus* as described previously [23]. It was purified by anion-exchange chromatography using a 5 ml High Q Econopac column (Bio-Rad Laboratories) and a linear gradient of 20 CV of TEAB (triethylammonium bicarbonate), pH 8.5, (50 mM–1 M) at 1 ml/min as described previously [28]. After freeze-drying, substrate quantification was performed using a NanoDrop spectrophotometer and using $\varepsilon_{GTP} = 12000\ mol^{-1} \cdot 1 \cdot cm^{-1}$.

CE of sugar nucleotides

CE was performed on a Beckman Gold instrument using the 32 Karat software and a 57 cm bare silica capillary. The initial conditioning of the capillary was performed by washing the capillary with 0.1 M HCl for 30 min at 20 psi (1 psi = 6.9 kPa), followed by 10 min of water. For sample analyses, the capillary was washed for 2 min with 200 mM Borax buffer, pH 9, the sample was injected by pressure for 4 s, separation was performed under 26 kV and detection was at 254 nm. The capillary was washed for 2 min with water, for 2 min with 0.1 M NaOH and for 2 min again with water between each run. Substrate conversion was estimated by integration of the surface areas under the substrate and product peaks using the 32 Karat software.

MS analyses

MS analyses of the sugar nucleotides were performed at the Dr Don Rix Protein Identification Facility, University of Western Ontario. All sugar nucleotides were analysed by LC-MS/MS (tandem MS). Separation was carried out with a Phenomenex Jupiter Proteo 90 A column (150 mm × 1.0 mm, 4 μm particle size) at a flow rate of 40 μl/min with a 1–50 % acetonitrile (with 0.1 % formic acid) gradient in 15 min. MS was performed on a Micromass Q-TOF (quadrupole–time-of-flight) spectrometer equipped with a Z-spray source operating in the negative ion mode (40 V, 80 °C) with a scan range 60–700 *m/z*.

MS analyses of the purified WcbK and WcaG enzymes were performed by MALDI (matrix-assisted laser-desorption ionization) using a 4700 Proteomics Analyzer (Applied Biosystems) in the linear positive-ion mode to confirm their size. The analyses were performed at the MALDI–MS facility of the University of Western Ontario as described previously [23].

Enzyme assays

Typically reactions were performed by incubating 50 ng–2 μg of enzyme with 0.1 mM substrate [GDP-*manno*-heptose prepared as described above or commercial GDP-mannose (Sigma)] in a final volume of 10 μl of 200 mM Tris/HCl buffer, pH 8.5, unless stated otherwise. Reactions were incubated for as little as 2 min to up to overnight at 37 °C. Specific conditions for each experiment are stated in the legends to the Figures. The reaction products were analysed by CE as described above. Large-scale reactions of 200 μl were prepared by a direct proportional increase of all components for MS analysis. In that case, the buffer used was volatile TEAB.

For determination of K_m, V_{max} and catalytic-centre activity, 11 reactions with various concentrations of substrate (0.2–1.2 mM) were set up in duplicate and incubated at 37 °C for reaction times (15 and 20 min for GDP-mannose, and 13 and 17 min for GDP-*manno*-heptose) that fell within the range of linearity of product formation over time and that allowed conversion of <10 % of the substrate for Michaelis–Menten analysis. The data are the average of two independent experiments and were calculated using the Lineweaver equation. All reactions were flash-frozen in a solid CO_2 ethanol bath and were run individually immediately after thawing. Protein concentrations were determined using the Bio-Rad protein assay reagent according to the manufacturer's directions with BSA as a standard.

NMR spectroscopy

Large-scale reactions were performed using 1 μmol of GDP-mannose, 1.5 μmol of NADH, 14 μg of WcbK or 5 μg of DmhA, and 16 μg of WcaG in 1.5 ml of 0.2 M TEAB, pH 8.5. The enzymes were added to the reactions as four equal aliquots over a 2 h period, and the reactions were left to incubate further overnight at 37 °C. The reactions were filtered through a 10 kDa cut-off ultrafiltration centrifugal device (Pall Filtron) to remove the enzymes, and the reaction products were purified by anion-exchange chromatography as described above. The purity of the fractions was monitored by CE. The purified products were freeze-dried repeatedly after resuspension in Milli-Q water (twice) and in ^2H_2O (four times).

All ^{1}H NMR data were collected with a Varian Inova 600 MHz NMR spectrometer at 25 °C. One-dimensional ^{1}H NMR spectra were collected using a 2 s presaturation pulse centred on the residual $^1H^2HO$ resonance. ^{1}H and ^{13}C assignments for the WcbK/WcaG reaction product were determined from a two-dimensional ^{1}H TOCSY experiment [29], using a 6 kHz spinlock for 256 complex increments and a natural abundance ^{1}H-^{13}C HSQC (heteronuclear single-quantum coherence) experiment [30,31]. All spectra were processed using VnmrJ 2.1B software and ^{1}H and ^{13}C chemical shifts referenced to DSS (2,2-dimethylsilapentane-5-sulfonic acid) at 0.00 p.p.m.

Structural modelling

Structural modelling of WcbK and its *Burkholderia pseudomallei* and *Y. pseudotuberculosis* homologues $WcbK_{BP}$ and DmhA was performed using Swiss-Model (http://swissmodel.expasy.org) in

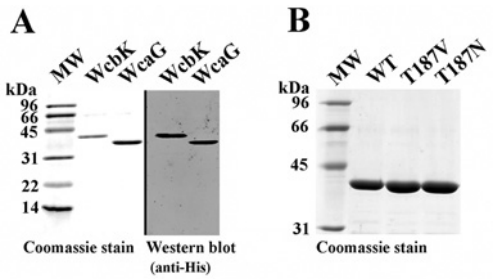

Figure 2 Expression and purification of WcbK and WcaG as determined by SDS/PAGE

(**A**) Analysis of purified wild-type WcbK and WcaG by Coomassie Blue staining and anti-His Western blotting. Both proteins were detected at the expected molecular masses of ~40.5 and 36.5 kDa respectively. (**B**) Coomassie Blue staining of purified T187N and T187V mutants alongside wild-type (WT) WcbK. The point mutations did not result in any differences in terms of yield, solubility and purity of WcbK. MW, molecular-mass markers.

the automatic mode. This led to automatic selection of the structures of GDP-mannose dehydratases from *Pseudomonas aeruginosa* (GMD, GDP-D-mannose 4,6-dehydratase; PDB code 1RPN) [32] or *Arabidopsis thaliana* (Mur1, PDB code 1N7G) [33] as a template. When needed, modelling was also performed in the 'constrained' mode using the GMD structure as a template. The models were visualized and aligned using PyMol (http://www.pymol.org). Residues involved in substrate binding in Mur1 were identified using the Ligand-Protein contacts software [34] (http://bip.weizmann.ac.il/oca-bin/lpccsu) and the accessible surface area in the binding site was calculated using the VADAR software [35] (http://vadar.wishartlab.com/). Matching residues constituting the binding sites in the GMD, WcbK and DmhA homologues were identified via sequence alignments and structural modelling. The accessible surface areas of these binding sites were also calculated using VADAR.

RESULTS

Expression and purification of WcbK and WcaG

Both WcbK and WcaG could be overexpressed in *E. coli* BL21(DE3)pLysS at high yield and in a soluble N-terminal His_6-tagged form using the pET system. They were purified to near-homogeneity in a single step of nickel-chelation-affinity chromatography, and migrated on SDS/PAGE gels at the expected size of 40.5 kDa and 36.5 kDa for WcbK and WcaG respectively (Figure 2A). The overexpressed proteins reacted readily with the anti-His antibody, thereby verifying their identity. Peaks of the expected sizes were also obtained for each enzyme by MALDI–MS analysis (results not shown). Cross-linking experiments showed that WcbK formed dimers and tetramers in solution (results not shown). The dimers were also observed by MALDI–MS and are consistent with published structural data from similar GDP-mannose dehydratases [32,36]. In contrast, WcaG did not oligomerize under the conditions tested by cross-linking and no oligomers were detected by MALDI–MS (results not shown).

WcbK uses GDP-*manno*-heptose as a substrate

Incubation of GDP-*manno*-heptose with WcbK led to the appearance of a new product (called P1) that migrated slightly upstream of the heptose substrate peak (peak H) by CE (Figure 3A, compare trace a with traces c and d). Degradation of P1 into GDP (migrating as peak P2 at 12 min; not shown), was also noted for long incubation times. Upon co-injection on the CE, product P1

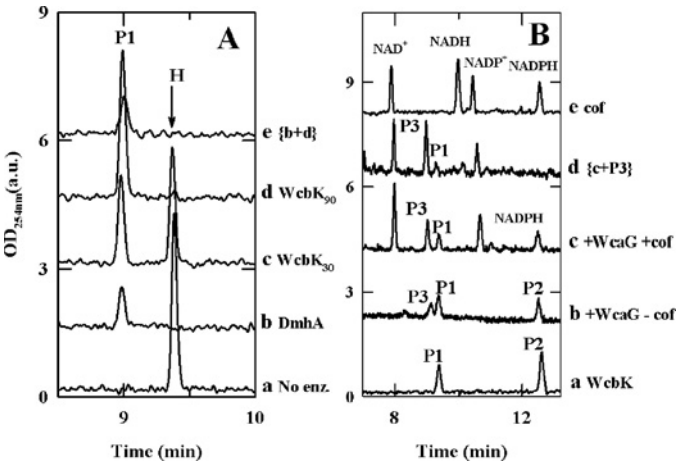

Figure 3 CE analysis of the reaction product obtained upon incubation of WcbK and WcaG with GDP-*manno*-heptose

(**A**) Analysis of the WcbK reaction product and comparison with the DmhA product. Incubation of WcbK with GDP-*manno*-heptose leads to the formation of a new product (P1) that co-migrates with the DmhA reaction product upon co-injection on CE. The reactions contained 50 ng of enzyme and 0.1 mM heptose (H). Trace a: heptose only. Trace b: DmhA control, 30 min reaction. Trace c: WcbK, 30 min reaction. Trace d: WcbK, 90 min reaction. Trace e: co-injection of samples from traces b and d. (**B**) Analysis of the WcbK/WcaG reaction product. The formation of a new product (P3) that migrates upstream of the oxo-deoxy-heptose peak (P1) produced by WcbK was observed upon addition of WcaG. This product co-migrated with purified GDP-6-deoxy-*manno*-heptose (trace d). Limited catalysis could occur in the absence of cofactor (cof; trace b). When cofactors [NAD(P)H] were supplied (trace c), catalysis was enhanced and formation of oxidized cofactors $NAD(P)^+$ was observed, indicating that WcaG can use either cofactor. However, the fact that all of the NADH was consumed and some NADPH remained indicates that NADH may be the preferred cofactor for WcaG. Reactions were performed by incubating 50 ng of WcbK with 0.05 mM heptose for 3 h, followed by incubation with 4 μg of WcaG and the appropriate cofactor. This large amount of WcaG was necessary to observe catalysis in the absence of exogenous cofactor. However, 250 ng of WcaG sufficed to observe catalysis in the presence of cofactor. Trace a: WcbK only. Trace b: WcbK and WcaG, no cofactor. Trace c: WcbK and WcaG, with NAD(P)H cofactors. Trace d: sample from trace c to which purified GDP-6-deoxy-*manno*-heptose (P3) was added. Trace e: control for cofactors. a.u., arbitrary units; enz, enzyme; OD, *A* (absorbance).

co-migrated with the reaction product of DmhA (Figure 3A, traces b and e), which was previously identified as GDP-4-oxo,6-deoxy-D-*lyxo*-heptose [23] (Figure 1C). This suggests that WcbK and DmhA make the same reaction product.

WcaG reduces the heptose-based reaction product of WcbK

WcaG converted the P1 reaction product obtained upon incubation of GDP-*manno*-heptose with WcbK into a new product (peak P3) that co-migrated with the product P3 generated by DmhA/DmhB (Figures 3B and 1D). Catalysis performed in the presence of the exogenous cofactor NAD(P)H was accompanied by consumption of NAD(P)H and formation of $NAD(P)^+$, indicating that catalysis involved a reduction step (Figure 3B, trace c) and that WcaG could use either cofactor. Although NADH was entirely used up under the conditions tested, a significant amount of NADPH was left, suggesting that NADH may be the preferred cofactor. Limited catalysis could also occur in the absence of exogenous cofactor (Figure 3B, trace b). This suggested that WcaG harboured a bound cofactor that was not lost during nickel chromatography purification. This cofactor supported a first round of catalysis and was not released from the enzyme during the process, since no $NAD(P)^+$ peak was observed on CE traces (Figure 3B, trace b). In the absence of exogenous reduced cofactor, there was no possibility for replenishment of the enzyme, so catalysis did not

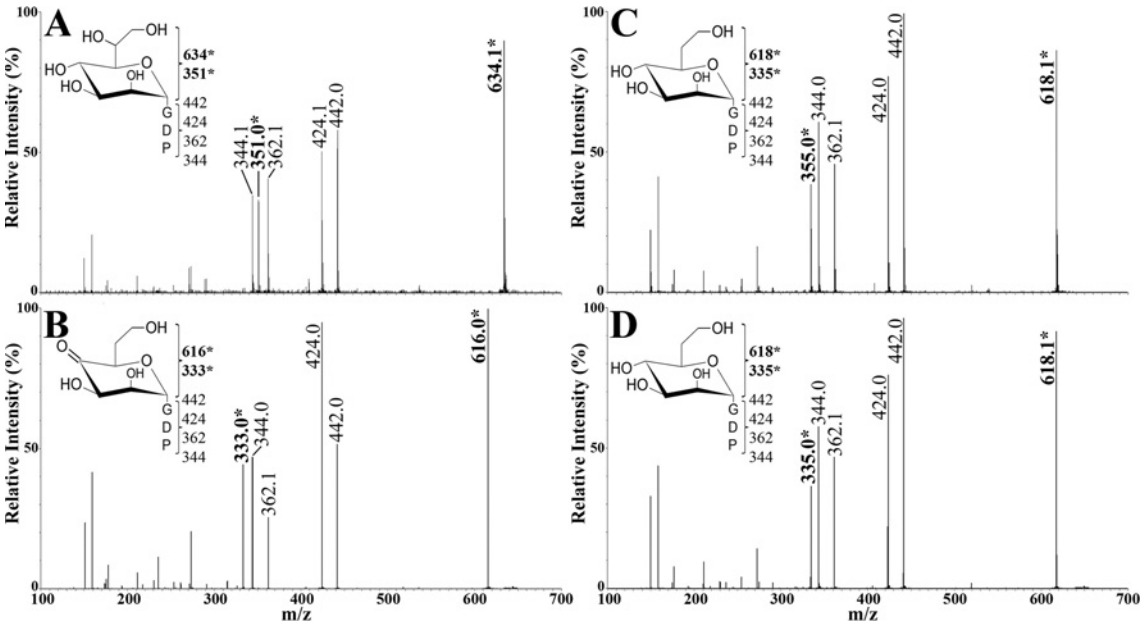

Figure 4 MS analysis of the WcbK and WcaG reaction products obtained with GDP-*manno*-heptose

All spectra shown are MS/MS spectra. Fragments highlighted in bold and with an asterisk include the heptose ring. (**A**) GDP-*manno*-heptose reference spectrum. (**B**) Spectrum for the WcbK reaction product P1. (**C**) Spectrum for the WcbK/WcaG reaction product P3. (**D**) Spectrum for the DmhA/WcaG reaction product P3.

proceed to completion. Therefore a significant portion of the WcbK reaction product P1 degraded into P2. The percentage conversion observed in the absence of extra cofactor was consistent with the high enzyme/substrate molar ratio used for these experiments.

Dialysis of purified WcaG resulted in loss of activity, which could be restored partly upon addition of NAD(P)H (results not shown). This indicates that the cofactor was lost upon dialysis of WcaG and may also play a role in stabilizing its structure. More activity was restored upon addition of NADH than NADPH (results not shown), indicating that although WcaG can use either cofactor, NADH is the optimal one. This is consistent with the results in Figure 3(B), trace c, that also suggested that NADH was the favoured cofactor.

Identity of the reaction products P1 and P3 generated upon catalysis of GDP-*manno*-heptose by WcbK and WcaG

LC-MS/MS analysis of the WcbK reaction product showed the presence of a product at *m*/*z* 616 (Figures 4A and 4B), which corresponds to the loss of 18 mass units compared with the original substrate (detected at *m*/*z* 634). This is consistent with the formation of the expected 4-oxo, 6-deoxy-heptose intermediate. Also, the MS/MS of the parent peak at *m*/*z* 616 yielded a fragment at *m*/*z* 333, which corresponds to the dehydrated heptose ring. The MS/MS pattern also showed fragments previously assigned to the GDP moiety of the molecule [23], which is not affected by catalysis.

LC-MS/MS analyses indicated that catalysis of GDP-*manno*-heptose by the WcbK/WcaG enzyme pair leads to the formation of a product with *m*/*z* 618, as expected for GDP-6-deoxy-heptose (Figure 4C). Its MS/MS pattern was identical with that observed for GDP-6-deoxy-*manno*-heptose (P3; Figure 3B) obtained with DmhA/DmhB.

The WcbK heptose-based reaction product can be used by DmhB

A C3 epimerization step is necessary to form the 6-deoxy-*altro*-heptose present in the capsule of *C. jejuni* strain 81-176. We previously demonstrated by NMR that the heptose configuration was retained in the DmhA/DmhB pathway, as DmhA and DmhB use and release sugars in the D-*manno* configuration [23]. Therefore, to further investigate whether WcbK could be involved in the C3 epimerization process, we tested whether its reaction product could be used by DmhB, with the premise that a C3-epimerized product would probably not be readily used by DmhB.

When the reductase DmhB was added to WcbK/GDP-*manno*-heptose reactions, conversion of the WcbK product (P1) into a new product (P3) was observed (Figure 5A, trace c, peak P3). This WcbK/DmhB product P3 co-migrated with the GDP-6-deoxy-*manno*-heptose generated by DmhA/DmhB (Figure 5A, traces e–g). Although this does not exclude the presence of isomers, this suggests that the WcbK reaction product comprises the regular 4-oxo, 6-deoxy-*lyxo* intermediate used by DmhB.

WcaG reduces the heptose-based DmhA reaction product

To further probe whether WcbK supplies a C3-epimerized product to WcaG, or if WcaG uses a non-epimerized substrate (in *manno* configuration, as produced by DmhA) and could epimerize it concomitantly with the reduction reaction, we tested whether WcaG could also reduce the GDP-4-oxo-6-deoxy-*manno*-heptose produced by DmhA. A product was readily obtained (Figure 5B, trace c) and it co-migrated with the DmhA/DmhB reaction products (Figure 5B, traces d and e). The DmhA/WcaG product was detected at *m*/*z* 618 by MS, as expected for a oxo, 6-deoxy derivative, and its MS/MS fragmentation pattern was identical with that of the DmhA/DmhB reaction product reported previously (Figure 4D) [23]. Collectively, these results suggest that WcbK/WcaG

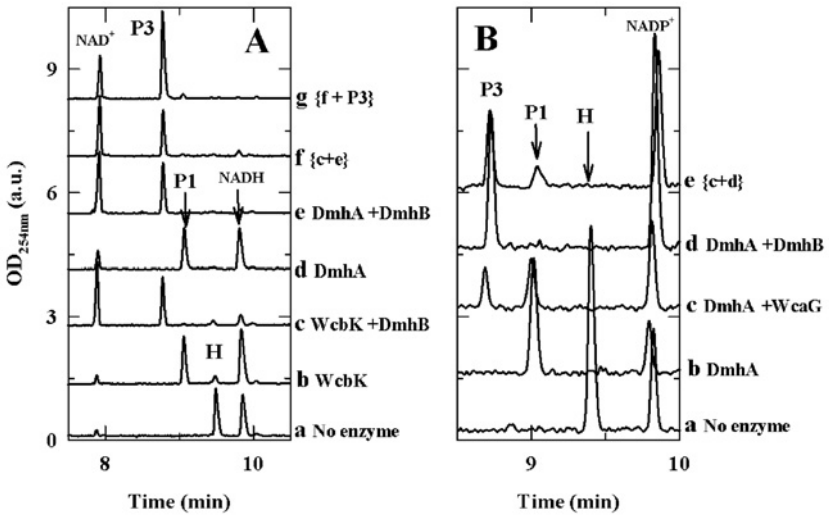

Figure 5 CE analysis showing that WcbK and DmhA, or WcaG and DmhB, can be used interchangeably for catalysis of GDP-*manno*-heptose

The reactions were performed in the presence of cofactors [NADH in (**A**) and equimolar mixes of NADPH and $NADP^+$ in (**B**)] since reduced cofactors were required for maximal activities of the reductases. The cofactor peaks (reduced and oxidized forms) also served as internal standards to facilitate peak alignments. (**A**) The WcbK reaction product can be used by DmhB. Incubation of DmhB and WcbK with GDP-*manno*-heptose led to the formation of a new product that co-migrated with the P3 product obtained upon incubation with DmhA and DmhB, and also co-migrated with purified DmhA/DmhB reaction product. The reactions contained 50 ng of WcbK, 50 ng of DmhA and/or 250 ng of DmhB, as needed, 0.2 mM of heptose (H) and 0.33 mM cofactor, and were incubated for 30 min. Trace a: heptose with NADH control. Trace b: reaction with WcbK only. Trace c: full reaction with WcbK and DmhB. Trace d: reaction with DmhA only. Trace e: full reaction with DmhA and DmhB. Trace f: co-injection of samples from traces c and e. Trace g: co-injection of sample from trace f with purified P3 product. (**B**) WcaG can use the DmhA reaction product. The reactions contained 50 ng of DmhA, 250 ng of WcaG, 0.1 mM of heptose (H) and 0.1 mM cofactor. They were incubated for 2 h. Trace a: heptose and $NADP^+$ control, no enzyme. Trace b: DmhA only. Trace c: DmhA and WcaG. Trace d: DmhA and DmhB. Trace e: co-injection of samples from traces c and d. As observed with WcbK, WcaG was able to use the DmhA reaction product and to convert it into a new product (P3) that co-migrated with the GDP-6-deoxy-*manno*-heptose generated by DmhA and DmhB. a.u., arbitrary units; OD, *A* (absorbance).

enzymes do not carry out the expected C3 epimerization of the substrate.

WcbK also uses GDP-mannose as a substrate

To test whether WcbK is specific for GDP-*manno*-heptose, or can also use hexoses as substrates, its ability to use GDP-mannose was investigated. Catalysis of GDP-mannose proved to be very efficient, with formation of a new product migrating ~1 min downstream of GDP-mannose (Figure 6A, peak P1′). This product represents potentially GDP-4-oxo-6-deoxy-mannose on the basis of prior assignments [37]. This product was formed even with low amounts of enzyme, short incubation times, and upon incubation at low temperature. This indicates that GDP-mannose is a good substrate for WcbK. This is in contrast with DmhA, which only used the GDP-mannose substrate very poorly [23]. Over time and upon exposure to high temperature, product P1′ degraded into product P2′ (Figure 6A), which we identified previously as GDP. [23]

LC-MS/MS analysis of the GDP-mannose/WcbK reaction product showed the presence of a product at *m*/*z* 586 (Figures 7A and 7B), that is 18 mass units lower with the original substrate (*m*/*z* 604). The MS/MS of the parent peak at *m*/*z* 586 yielded a fragment at *m*/*z* 303 that corresponds to the dehydrated mannose ring. These MS results are consistent with the expected formation of a 4-oxo-6-deoxy intermediate.

The WcbK mannose-based reaction product can be used interchangeably by DmhB or WcaG

CE analyses demonstrated that DmhB and WcaG can reduce the mannose-based dehydration product of WcbK (Figures 6B and 6C). With either enzyme, the product obtained co-migrated with the P3′ DmhA/DmhB reaction product (Figure 6B, traces d–f). This product migrates very closely to the GDP-mannose substrate, but control reactions performed in the absence of WcaG or DmhB showed that the substrate had been totally consumed by WcbK under the conditions used (Figures 6B and 6C, traces b), thereby confirming that the peak observed corresponds to a new reaction product generated by WcaG or DmhB. Although DmhB requires cofactor for function as demonstrated previously [23], catalysis by WcaG was observed both in the presence or absence of exogenous cofactors. In the absence of exogenous cofactors (Figure 6C, trace c), catalysis was incomplete as some WcbK product (P1′, 40 %) was still present and a significant amount of P1′ was degraded into GDP (peak P2′, 20 %). Product P3′ was nevertheless clearly detected (30 %). When the reactions were performed in the presence of NADH (Figure 6C, trace d), catalysis with WcbK/WcaG was complete as hardly any WcbK product P1′ was left, no degradation of P1′ into P2′ was observed, and all of the cofactor was transformed into NAD^+ (trace d). In contrast, even in the presence of cofactor, catalysis of the WcbK product by DmhB was inefficient, with significant degradation of P1′ into P2′ (Figure 6B, trace c).

To identify the final WcbK/WcaG reaction product P3′, LC-MS/MS analyses were performed on reactions prepared in the absence of cofactor but with large amounts of enzyme, to ensure that they had reached completion. The product was detected at *m*/*z* 588 and its MS/MS pattern was identical with that obtained with P3′ formed by DmhA/DmhB (Figure 7C).

WcaG reduces the mannose-based DmhA reaction product

As observed with the WcbK/WcaG or WcbK/DmhB pairs, incubation of GDP-mannose with DmhA/WcaG led to the formation of the expected P3′ product detected as a right shoulder

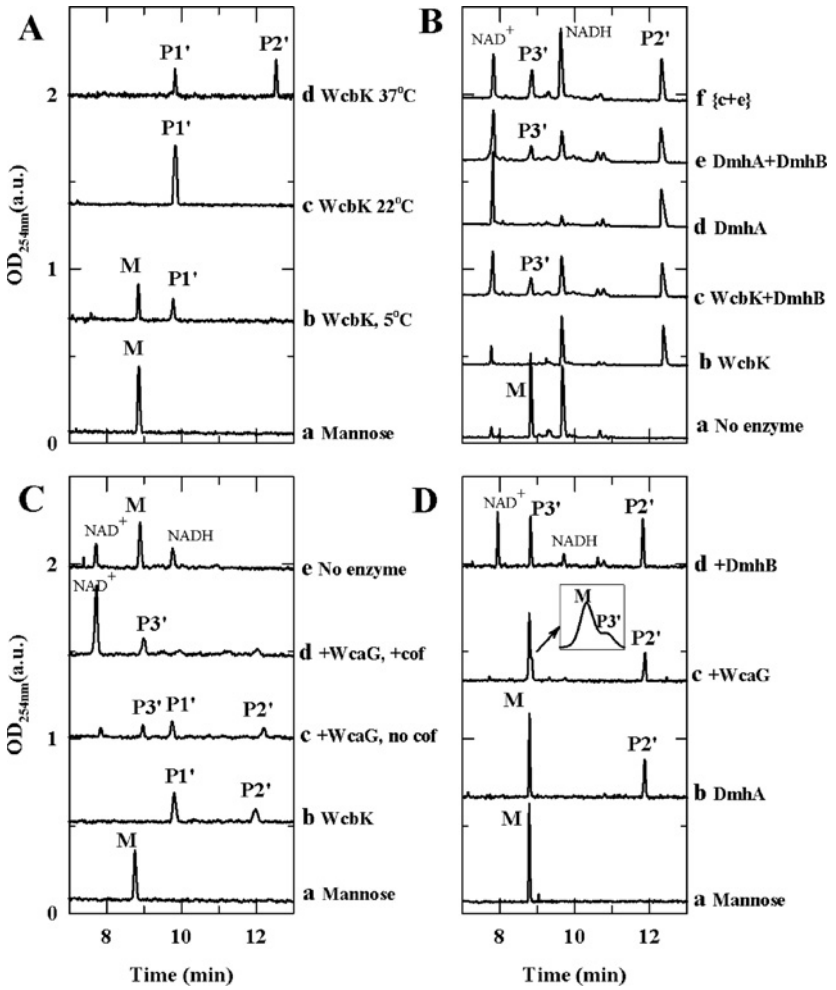

Figure 6 CE analysis of the reaction products obtained upon incubation of WcbK and WcaG with GDP-mannose

(**A**) Formation of a new product (P1′) that migrates downstream of the mannose (M) substrate upon incubation with WcbK. The reactions typically contained 1 μg of WcbK and 0.1 mM GDP-mannose (M). They were incubated for 2 h at 5 °C (traces a and b), 22 °C (trace c) or 37 °C (trace d). WcbK was very active even at low temperatures. Using a lower temperature allowed stabilization of the temperature-sensitive product P1′. At the higher temperature, product P1′ degraded into product P2′, which we identified previously as GDP by MS analysis. (**B**) Incubation of WcbK and DmhB with GDP-mannose leads to the formation of the same P3′ product as formed in reactions with DmhA and DmhB. The reactions typically contained 1 μg of WcbK or DmhA, 2 μg of DmhB and 0.33 mM GDP-mannose (M). They were incubated overnight to account for the low efficiency of catalysis of DmhB on mannose-based substrates. The long incubation resulted in significant degradation of the DmhA and WcbK products into P2′. Trace a: GDP-mannose control. Trace b: reaction with WcbK. Trace c: reaction with WcbK and DmhB. Trace d: reaction with DmhA only. Trace e: reaction with DmhA and DmhB. Trace f: co-injection of samples from traces c and e. (**C**) The WcbK reaction product P1′ can be used by WcaG to form product P3′ and limited catalysis can occur in the absence of exogenous cofactor (cof). WcbK (1 μg) was incubated with 0.1 mM GDP-mannose for 1 h at 22 °C to limit P1′ degradation. WcaG (2 μg) was then added to the reaction along with cofactor or not, and incubation was allowed to proceed for 1 h at 37 °C. Trace a: GDP-mannose control. Trace b: WcbK only. Trace c: WcbK and WcaG, no cofactor. Trace d: WcbK and WcaG, with cofactor NADH. Trace e: control trace for cofactors (NADH and NAD^+) and GDP-mannose. (**D**) WcaG can also use the DmhA mannose-based product as a substrate (trace c), and forms the same P3′ product as obtained with the DmhA/DmhB pair (trace d). Reactions were as indicated in (**C**) except that DmhA was used instead of WcbK. Trace a: GDP-mannose control. Trace b: DmhA only. Trace c: DmhA and WcaG. Trace d: DmhA and DmhB. DmhA is poorly active on GDP-mannose, therefore a large leftover peak of GDP-mannose was observed. The product P3′ formed upon further addition of WcaG migrates as a right-hand shoulder off the mannose peak, similar to what was previously observed for DmhA/DmhB.

off the GDP-mannose peak (Figure 6D). This new peak had the expected size (*m*/*z* 588) and fragmentation pattern in MS analyses (Figure 7D). Therefore WcaG is also able to reduce the DmhA mannose-based reaction product.

Comparative NMR spectroscopy analysis of the WcbK/WcaG and DmhA/WcaG reaction products

As mentioned above, the DmhA/DmhB pathway generates GDP-6-deoxy-*manno*-heptose, whereas 6-deoxy-*altro*-heptose is found in the capsule of *C. jejuni* strain 81-876. It is not known whether WcbK, WcaG or another unidentified enzyme are responsible for the required change of sugar configuration. Although the heptose-based and mannose-based products generated by WcbK and WcaG appear identical with the DmhA and DmhB products by CE and MS analyses, we cannot exclude the presence of isomers in WcbK/WcaG reactions at this stage. Differences of reactivity of DmhB on the mannose dehydration products of WcbK and DmhA also suggest potential differences in stereochemistry of the products. Therefore the reaction products needed to be compared by NMR spectroscopy.

Considering the difficulty in producing the GDP-*manno*-heptose substrate in amounts suitable for NMR analyses, NMR experiments were carried out using GDP-mannose, as WcbK and WcaG readily catalyse conversion of this substrate (Figure 8). The spectrum of the WcbK/WcaG product compared with the spectrum of the starting material GDP-mannose clearly indicated the occurrence of C6 dehydration. Namely, a new ^{1}H signal was observed at 1.25 p.p.m. (Table 2) in the WcbK/WcaG product that was coupled to H5 on the basis of ^{1}H-TOCSY data. The ^{13}C shift

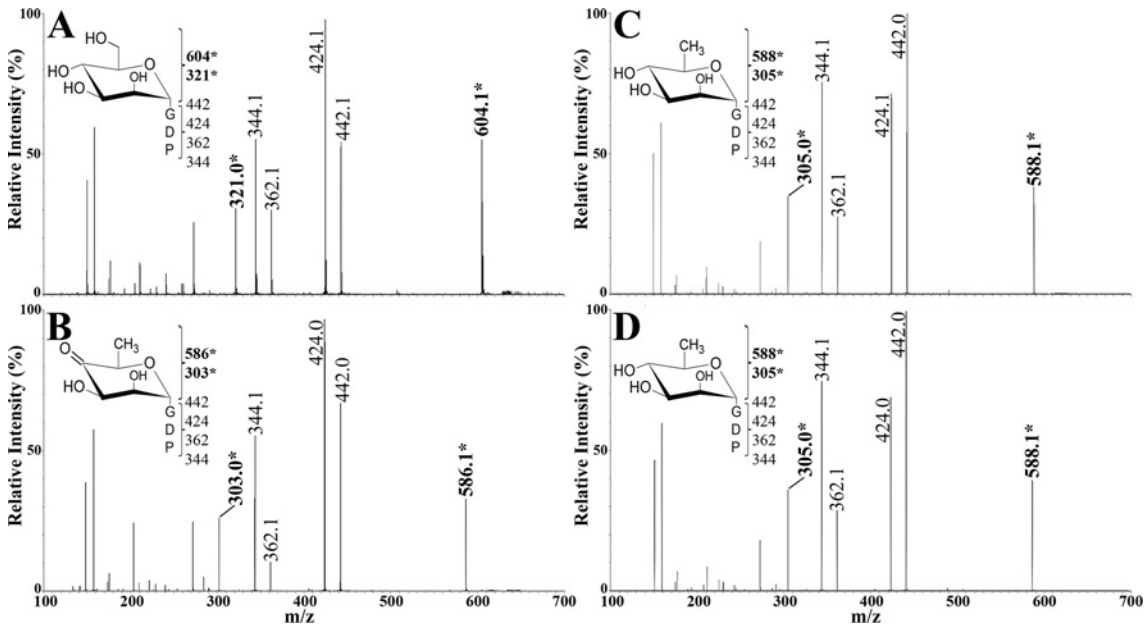

Figure 7 MS analysis of the WcbK and WcaG reaction products obtained with GDP-mannose

All spectra shown are MS/MS spectra. Fragments highlighted in bold and with an asterisk include the heptose ring. (**A**) GDP-mannose reference spectrum. (**B**) Spectrum for the WcbK reaction product P1′. (**C**) Spectrum for the WcbK/WcaG reaction product P3′. (**D**) Spectrum for the DmhA/WcaG reaction product P3′.

for this resonance (19.7 p.p.m.) identified from ^{1}H-^{13}C HSQC data indicated that this was a CH_3 group at C6. Concomitantly there was a disappearance of ^{1}H signals for H6 from GDP-mannose at 3.74 and 3.85 p.p.m. Similar observations have been made for the ^{1}H and ^{13}C chemical shifts of the C6 methyl signal for GDP-rhamnose, the C6 dehydration product of GDP-mannose [38]. In addition, a large chemical shift change, from 3.67 to 3.41 p.p.m., was noted for H4 in the WcbK/WcaG product as a result of hydroxy removal at C6. A similar change in chemical shift for H4 occurs upon dehydration at C6 of GDP-glycero-*manno*-heptose by DmhA [23], reflecting the change in environment at H4 from removal of the alcohol group. Collectively, these results demonstrate the occurrence of C6 dehydration.

The chemical shifts and $^{3}J_{HH}$ coupling constants for the WcbK/WcaG P3′ reaction product appeared nearly identical with the DmhA/WcaG P3′ reaction product, indicating that WcbK does not have any epimerization activity (Figure 8). Although this does not allow any conclusions about the potential epimerization activity of WcaG, we could not generate enough DmhA/DmhB product for comparison purposes owing to the poor catalysis of the DmhA mannose-based substrate by DmhB. However, the NMR spectra showed large ^{1}H,^{1}H coupling constants (>9 Hz) between H3, H4 and H5, consistent with their *trans* arrangement around the sugar ring (Table 2). Furthermore, the data were very similar to the published GDP-rhamnose spectrum [38–40] whereby GDP-rhamnose is the direct C6 dehydration product of GDP-mannose obtained via the activity of a non-epimerizing GDP-mannose dehydratase and reductase pair. This indicates that the purified reaction products analysed are all identical and have retained the *manno* configuration.

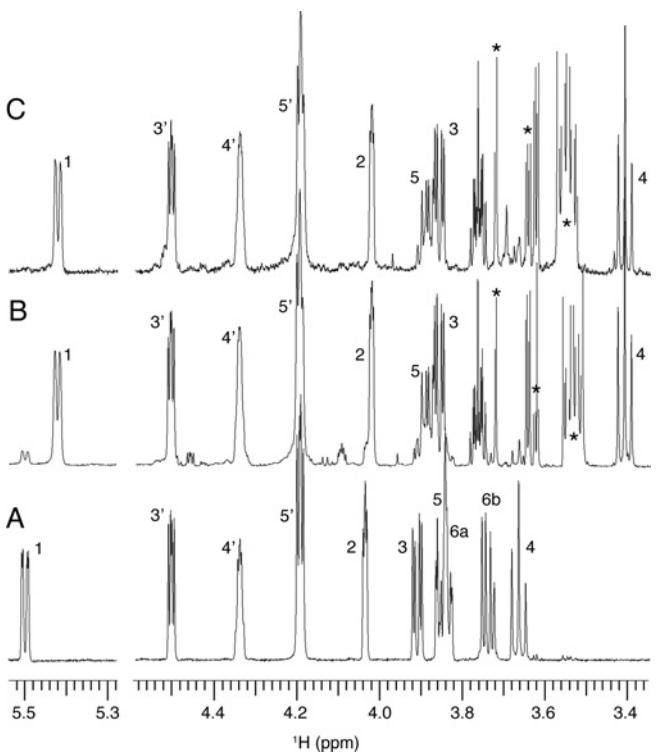

Figure 8 ^{1}H NMR spectra of the WcbK/WcaG and DmhA/WcaG reaction products

Selected regions of the 600 MHz ^{1}H NMR spectra for GDP-mannose (**A**) and the P3′ products from DmhA/WcaG (**B**) and WcbK/WcaG (**C**) enzyme reactions. Each spectrum shows the ^{1}H assignments of the sugar ring (1–5) and ribose (3′–5′) protons based on ^{1}H TOCSY experiments. The 1′ and 2′ protons from the ribose portion of the molecule were assigned and observed in different regions of the spectrum (not shown). In (**A**), peaks 6a and 6b correspond to the two protons of c6 of GDP-mannose. In (**B**) and (**C**), the H6 methyl group is found at 1.25 p.p.m. and is not shown in the spectra. Peaks labelled * result from small buffer impurities. The spectral regions are not scaled identically.

Physico-kinetic parameters for the activity of WcbK

No exogenous cofactor was required for, nor increased, catalysis of the heptose or hexose substrates by WcbK. On the basis of the known reaction mechanism for C6 dehydration, this suggests that WcbK carries a tightly bound NAD(P)$^{+}$ molecule. This was

Table 2 ^{13}C and ^{1}H NMR data for GDP-mannose and DmhA/WcaG and WcbK/WcaG reaction products

n.a., not applicable; n.d., not determined; n.r., not reported.

Compound or reaction		H Chemical shifts (p.p.m.) and coupling constants (Hz)					
		H1	H2	H3	H4	H5	H6
GDP-mannose*	^{1}H	5.50	4.04	3.91	3.67	3.85	3.74/3.85
	$^{3}J_{HH}$ ($^{3}J_{HP}$)	1.8 (7.1)	3.4	9.9	9.8	5.3	n.a.
	^{13}C	99.3	73.1	72.7	69.4	76.5	63.6
DmhA/WcaG product*	^{1}H	5.42	4.02	4.86	3.41	3.89	1.25
	$^{3}J_{HH}$ ($^{3}J_{HP}$)	2.2 (7.1)	3.4	9.9	9.8	6.3	n.d.
	^{13}C	99.1	73.1	72.5	74.7	72.6	19.5
WcbK/WcaG product*	^{1}H	5.42	4.02	3.86	3.41	3.89	1.25
	$^{3}J_{HH}$ ($^{3}J_{HP}$)	1.9 (7.5)	3.4	9.8	9.7	6.4	n.d.
	^{13}C	99.1	73.2	72.4	74.8	72.4	19.7
GDP-α-D-rhamnose†	^{1}H	5.43	4.03	3.86	3.42	3.89	1.25
	$^{3}J_{HH}$ ($^{3}J_{HP}$)	1.2 (7.6)	3.5	9.7	9.8	6.1	n.r.
	^{13}C	97.2	71.2	70.4	72.8	70.4	17.6

*Chemical shifts referenced to internal DSS standard: $^{1}H = 0.00$ p.p.m. Only chemical shifts from the sugar portions of the compounds are reported.
†Chemical shifts referenced to internal acetone standard: $^{1}H = 2.225$ p.p.m, $^{13}C = 31.07$ p.p.m. Data from King et al. [38].

demonstrated by the fact that the presence of NAD^+ was observed by MS analysis of the supernatant obtained after heat denaturation of WcbK (results not shown).

As determined using GDP-mannose as a substrate, the activity of WcbK was optimal at pH 8.5–9.0 and between 37 and 50 °C (results not shown). The slightly thermophilic character of WcbK could reflect the adaptation of *C. jejuni* for optimal growth at 42 °C, and is consistent with the fact that the capsule and its heptose modification are functionally important *in vivo*.

Kinetic parameters were determined under the optimal conditions described above for both the heptose and hexose substrates. As summarized in Table 3, the K_m values for GDP-*manno*-heptose and GDP-mannose were of the same order of magnitude and indicated relatively strong affinity of WcbK for both substrates. They were comparable with values previously obtained for DmhA. Although the catalytic efficiency for GDP-*manno*-heptose was 70-fold lower for WcbK than for DmhA, the k_{cat} and catalytic-centre activity k_{cat}/K_m were much higher for GDP-*manno*-heptose than for GDP-mannose, indicating preference of WcbK for the heptose-based substrate versus the hexose, as seen for DmhA. For GDP-mannose, the catalytic-centre activity k_{cat}/K_m was ~3-fold higher for WcbK than for DmhA. This, along with the higher enzyme concentrations obtainable for WcbK than for DmhA, explains that the product P1′ could be observed with WcbK but not with DmhA [23].

Physico-kinetic parameters for WcaG

Using the WcbK/GDP-mannose reaction product as a substrate, we determined that WcaG functioned optimally at 37 °C and in the pH range 8.0–9.5 (results not shown). The absolute K_m and V_{max} of WcaG could not be determined because of the unstable character of the oxo substrates.

Structural modelling of the three heptose dehydratases

As mentioned earlier, 6-deoxyheptoses of various configurations are found in *Y. pseudotuberculosis* (D-*manno*), *C. jejuni* 81-176 (D-*altro*) and *B. pseudomallei* (L-*talo*). Our biochemical analysis revealed different heptose versus hexose preference patterns for the *Y. pseudotuberculosis* DmhA and the *C. jejuni* 81-176 WcbK (called $WcbK_{CJ}$ in this section for clarity) [23], as well as different catalytic efficiencies on GDP-*manno*-heptose. Therefore the structures of the dehydratases found in each species were modelled to identify residues potentially involved in determining their substrate specificity.

Structural modelling of $WcbK_{CJ}$, $WcbK_{BP}$ and DmhA was performed using SwissModel. A single model was obtained for each protein in the automatic mode, which used the structure of the *P. aeruginosa* GDP-mannose dehydratase GMD (PDB code 1RPN) [32] for $WcbK_{BP}$ and DmhA, and used the structure of the *A. thaliana* GDP-mannose dehydratase Mur1 (PDB code 1N7G) [33] for $WcbK_{CJ}$. A model of $WcbK_{CJ}$ was also obtained upon selection of the *P. aeruginosa* GMD structure as a modelling template. The two models were virtually identical (results not shown). The only differences comprised a slightly longer helix (Val^{320}–Leu^{342}) with the Mur1-based model compared with the GMD-based model (Val^{320}–Lys^{336}), and a small stretch of four amino acids (Glu^{245}–Lys^{248}) that was predicted as a loop in the Mur1-based model, whereas it was predicted as a short helix in the GMD-based model. These differences are located remotely from the substrate-binding site. Since DmhA and $WcbK_{BP}$ were modelled with GMD as a template, the $WcbK_{CJ}$ model obtained with GMD was used for further comparisons of the three enzymes, as described below. Overall, the three models show a similar bilobal structure, one lobe consisting of a characteristic Rossmann fold important for cofactor binding, whereas the other is involved in GDP binding (Supplementary Figure S1 at http://www.BiochemJ.org/bj/439/bj4390235add.htm). Catalysis occurs presumably at the interface between both lobes as seen in GMD and Mur1. GMD is known to dimerize via the formation of a four-helix bundle involving helices a4 and a5 of each monomer [32]. These helices occupy the same positions in our models and probably support the dimerization of $WcbK_{CJ}$ that we observed via cross-linking and by MALDI–MS. GMD and Mur1 are also known to form tetramers via dimerization of dimers [32,33]. The global similar modelled tertiary structure of $WcbK_{CJ}$ and its observed tetramerization in cross-linking experiments indicate that this is also the case for $WcbK_{CJ}$, and probably for its homologues $WcbK_{BP}$ and DmhA.

Since Mur1 was previously co-crystallized with its cofactor and its reaction product GDP-rhamnose [33], the obtained models were all aligned on to the Mur1 structure to facilitate analysis of their modelled active sites (Supplementary Figure S1). GDP-rhamnose is the dehydration product of GDP-mannose, and is

Table 3 Kinetic parameters for the catalysis of GDP-*manno*-heptose and GDP-mannose by WcbK, and comparison with DmhA

Results are means ± S.D.

Enzyme	K_m (mM)	V_{max} (pmol · min^{-1})	Enzyme amount (pmol)	k_{cat} (min^{-1})	k_{cat}/K_m (min^{-1} · mM^{-1})
GDP-*manno*-heptose					
WcbK	0.92 ± 0.02	19.3 ± 3.3	0.3	62 ± 10	67 ± 11
DmhA*	0.23 ± 0.02	240 ± 30	0.2	1100 ± 140	4700 ± 140
GDP-mannose					
WcbK	0.79 ± 0.05	51.5 ± 2.9	31.1	1.66 ± 0.09	2.09 ± 0.14
DmhA*	0.32 ± 0.03	2.7 ± 0.4	11.1	0.25 ± 0.03	0.78 ± 0.06

*Results for DmhA were previously reported in Butty et al. [23].

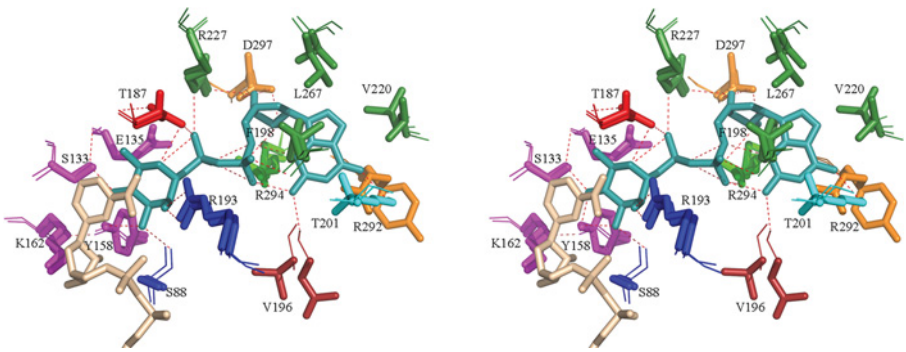

Figure 9 Stereo view of the modelled substrate binding site of WcbK

The model for the *C. jejuni* 81-176 WcbK was created using SwissModel and visualized with PyMol. The modelled structure of the WcbK substrate-binding site is shown overlayed with the active site of the GDP-mannose dehydratase Mur1 (PDB code 1N7G) that was co-crystallized with its cofactor (beige sticks) and GDP-rhamnose (light blue sticks). The hydrogen bonds between Mur1 and GDP-rhamnose are shown as red broken lines. The numbered amino acid residues correspond to WcbK. The side chains are shown as sticks and the main chains are shown as lines. Residues important for substrate and cofactor binding and catalysis are highlighted in colour as follows. The conserved catalytic serine/threonine, glutamic acid, tyrosine and lysine residues are in magenta. Residues involved in sugar binding and conserved in GDP-mannose and GDP-*manno*-heptose dehydratases are in dark blue. Residues involved in nucleotide (GDP) binding and conserved in all proteins are in green. All other coloured residues are different in the mannose dehydratases compared with the *manno*-heptose dehydratases, but are conserved within each category. See the text for details.

relevant to our present study since both DmhA and $WcbK_{CJ}$ can use GDP-mannose as a substrate. No crystal structure was available to proceed similarly with GDP-*manno*-heptose.

Residues potentially important for substrate binding and catalysis in the three GDP-*manno*-heptose dehydratases $WcbK_{BP}$, $WcbK_{CJ}$ and DmhA were identified in the modelled structures based on data obtained for the *P. aeruginosa* and *A. thaliana* GDP-mannose dehydratases GMD and Mur1 mentioned above, as well as for the *E. coli* GDP-mannose dehydratase [32,33,36]. These residues are presented for all proteins within the global protein structure in Supplementary Figure S1, and more specifically in a zoomed stereo view of the active site for $WcbK_{CJ}$ (Figure 9). The residues are also shown in sequence alignments of protein segments that define the substrate-binding site (Figure 10). The canonical serine/threonine, glutamic acid, tyrosine and lysine catalytic residues were conserved in all proteins, and were identified in similar positions in each structure model (magenta in Figure 9 and Supplementary Figure S1). A serine residue, known to coordinate both to the cofactor through its side-chain OH and to the rhamnose C3 OH group via its main-chain carbonyl, was conserved and occupied a similar position in all enzymes [Ser^{88} (dark blue) in $WcbK_{CJ}$ (Figure 9 and Supplementary Figure S1)]. Similarly, an arginine residue known to coordinate both the cofactor and the C2 OH of the rhamnose through its guanidinium side chain in mannose dehydratases was conserved both in sequence and position in the three heptose dehydratase models [Arg^{193} (dark blue) in $WcbK_{CJ}$ (Figure 9 and Supplementary Figure S1)]. This double coordination of the sugar and of the cofactor probably ensures proper positioning to facilitate hydride transfer from the sugar to the cofactor during catalysis.

In contrast, a conserved asparagine residue known to coordinate with the C6 OH of GDP-mannose [32,33] and with the β-phosphate of GDP via its amide side chain was replaced by a threonine residue in all heptose dehydratase models [Thr^{187} (red) in $WcbK_{CJ}$ (Figure 9 and Supplementary Figure S1)]. Although the polar character of the side chain is conserved by the asparagine/threonine substitution, the orientation of the threonine OH side chain is such that it cannot interact with the GDP phosphate and probably only interacts with the C7 OH group of the heptose substrate. No significant contact can be anticipated with the C6 OH in the heptose dehydratases on the basis of the structural models obtained (Figure 9 and Supplementary Figure S1). Consequently, a mannose substrate would not benefit from the additional fine-tuning of substrate positioning offered by this residue, which may explain the observed lower catalytic efficiency on such a substrate despite its ability to fit in the binding pocket. Therefore Thr^{187} appears to be a potential candidate determinant of substrate specificity in $WcbK_{CJ}$ and its homologues, namely allowing proper positioning of the heptose via its interaction with the side-chain OH. The presence of a threonine residue instead of the asparagine found in mannose dehydratases also allows accommodation of the larger heptose via the slightly smaller size of threonine.

```
Protein     AA# Sequence // AA# Sequence  // AA# Sequence
WcbK CJ     130 ICSSSEVY     156 SPYSISKIG    185 MGTHSGPRRSDVFFESTVAKQ
DmhA        129 VCSSSEVY     155 SPYSISKIG    184 MGTHTGPRRSDVFFESTVAKQ
WcbK BP     126 VCASSEVF     153 SPYAISKVG    182 MFTHTGPRRGDVFAESTFAKQ
Mur1        159 QAGSSEMF     183 SPYAASKCA    212 LFNHESPRRGENFVTRKITRA
GMD         123 QASTSEMF     147 SPYGVAKLY    177 LFNHESPLRGIEFVTRKVTDA
Structure       bbbb hhh         hhhhhhhhh                    hhhhhhhh
Area inter.      Sugar            Sugar            Sugar    Guanine

Protein     AA# Sequence         // AA# Sequence   // AA# Sequence
WcbK CJ     218 IKVGNLSSVRTFQDC     265 FKLPEVIDIL     290 EDRMRPIDAD
DmhA        217 LKVGNLASVRTFQDA     264 FKLPEVIELL     288 TDRLRPIDAD
WcbK BP     215 VKTGNLDSLRTFADV     258 CTVGQMLDTL     283 PERLRPIDAD
Mur1        244 LFLGNLQASRDWGFA     285 HTVEEFLDVS     310 QRYFRPAEVD
GMD         209 LRLGNVDAKRDWGFA     250 TTVRDMCQIA     275 PAFFRPAEVD
Structure                                hhhhhhhh       hhh
Area inter.          GDP    cat.          GDP            Guanine
```

Figure 10 Sequence alignment of protein sections comprising the conserved residues involved in substrate binding in GDP-*manno*-heptose and GDP-mannose dehydratases

WcbK CJ, *C. jejuni* 81-176 WcbK; WcbK BP, WcbK from *B. pseudomallei*; DmhA, GDP-*manno*-heptose dehydratase from *Y. pseudotuberculosis*; Mur1, GDP-mannose dehydratase from *A. thaliana*; GMD, GDP-mannose dehydratase from *P. aeruginosa*. AA#, number of the first amino acid of each segment in the protein sequence. The specific area of interaction of these residues within the sugar nucleotide (Area inter.) and the secondary structure adopted by these residues (b, β-sheet; h, α-helix) as determined by crystallography data for Mur1 and GMD and by structural modelling for the other proteins listed are indicated. 'cat.' indicates residues that do not have a direct interaction with the sugar nucleotide, but line up behind the catalytic residues, thereby probably playing a role in substrate binding by providing scaffolding for the catalytic pocket.

Not surprisingly, residues identified as important for binding of the GDP moiety of the substrate in mannose dehydratases were conserved or replaced by similar types of residues in the heptose dehydratases. This is the case for Arg^{227} (in $WcbK_{CJ}$), which coordinates to the ribose and the β-phosphate, Arg^{294}, which coordinates to both phosphates, and Phe^{198}, which replaces a conserved valine residue that interacts with the α-phosphate through its main-chain amide (all in green in Figure 9 and Supplementary Figure S1). Likewise, Leu^{267} and Val^{220} (green in $WcbK_{CJ}$) are located in positions occupied by similar hydrophobic amino acids in most dehydratases and that are known to delineate the back end of the GDP-binding pocket in mannose dehydratases [36].

Several differences were nevertheless observed in the GDP-binding area. For example, the conserved tyrosine/phenylalanine residue that interacts with the guanine base in GDP-mannose dehydratases [36] is replaced by arginine [Arg^{292} (orange) in $WcbK_{CJ}$ (Figure 9 and Supplementary Figure S1)], which may provide stabilization of the guanine via hydrogen bonding rather than ring stacking, but probably fulfils the same global role. In addition, a threonine residue [Thr^{201} (cyan) in $WcbK_{CJ}$] replaces a conserved lysine of mannose dehydratases, but is still anticipated to be able to fulfil the hydrogen bonding previously identified between the Nε of lysine and the guanine ring via its OH side chain. Finally, the conserved glutamic acid residue that interacts via its side-chain carbonyl with the GDP ribose is replaced by a conserved aspartatic acid [Asp^{297} (light orange) in $WcbK_{CJ}$]. The shorter side chain of the aspartatic acid residue could potentially pull the sugar deeper into the back of the sugar-binding pocket (GDP area), thereby allowing accommodation of the more bulky heptose at the front end of the binding pocket (heptose/mannose area).

The polar charged residues (Glu^{188} of GMD and Asn^{223} of Mur1; see Figure 10 and Supplementary Figure S1) not previously highlighted as being major contributors to substrate binding or catalysis, despite their conserved character, were replaced by a conserved valine residue [Val^{196} (dark red) in $WcbK_{CJ}$] in all heptose dehydratases. Although too far from the modelled substrate to participate in direct interactions, this smaller and hydrophobic residue present in the heptose dehydratases may allow less constraint in the substrate-binding pocket, and therefore may allow accommodation of the bulkier heptose substrate. This is one example of the variability observed within the sequences surrounding the conserved residues involved in substrate binding between the GDP-*manno*-heptose and GDP-mannose dehydratases. Overall, a sequence alignment of these sequences shows that these sequences were very conserved between the three heptose dehydratases, but differed slightly from the sequences found (and also conserved) in the hexose dehydratases (Figure 10).

These differences did not result in significant differences in the accessible surface area in the binding sites of the heptose dehydratases compared with the mannose dehydratases. Indeed, the accessible surface areas of 629 and 691 $Å^2$ (1 Å = 0.1 nm) calculated for the modelled binding sites of $WcbK_{CJ}$ and $WcbK_{BP}$ were very close to the values of 703 and 794 $Å^2$ calculated for GMD and Mur1 respectively. Only DmhA featured a slightly lower accessible surface area (585 $Å^2$) compared with all other proteins, reflecting a slightly more constricted binding site. Since the sequence conservation of substrate-binding-site residues between DmhA and $WcbK_{CJ}$ is 81 %, whereas it is only 42 % between Mur1 and $WcbK_{CJ}$, the lower accessible surface area of the DmhA substrate-binding site may result from a tighter packing of the binding site caused by surrounding residues not directly involved in substrate binding.

Of final note is that several of the residues involved in interactions with the substrate are part of unstructured loops (Figure 10), implying that, even in DmhA, flexibility of the binding site may be necessary to accommodate the substrate.

Role of Thr^{187} in substrate specificity of $WcbK_{CJ}$

The role played by Thr^{187} in substrate specificity of $WcbK_{CJ}$ was tested by site-directed mutagenesis. A T187N mutant was generated to mimic the situation observed in GDP-mannose dehydratases. A T187V mutant where threonine is replaced by a residue of similar size and shape was also generated to test whether the presence of threonine alleviates a simple steric hindrance problem whereby the larger asparagine residue may restrict the ability of GMD homologues to use heptose, or whether the polarity of the threonine side chain is important for interactions with the substrate.

The two mutants could be overexpressed and purified to near-homogeneity under the same conditions as the wild-type WcbK (Figure 2B). Time course experiments performed with various enzyme concentrations showed drastically reduced catalysis of GDP-*manno*-heptose by either mutant compared with wild-type enzyme (Figure 11A). This demonstrated that the Thr^{187} residue is important either in binding or catalysis of the GDP-*manno*-heptose substrate, and that both steric hindrance and side-chain polarity are important factors for fruitful catalysis. The fact that the T187V mutant was slightly more impaired than the T187N mutant suggests that proper positioning of the substrate via interaction through the polar threonine side chain is important for catalysis. This is also reflected by the fact that the threonine/valine mutant could hardly catalyse conversion of GDP-mannose, despite the larger binding pocket (Figure 11B). Note that these results were obtained using the same amounts of wild-type and mutated enzymes. However, significant levels of catalysis could be obtained with GDP-*manno*-heptose if larger concentrations of mutated enzymes were used, therefore eliminating the possibility that the relatively poor catalysis observed compared with the wild-type enzyme was due to major conformational changes of the enzyme upon introduction of the T187V/N mutations.

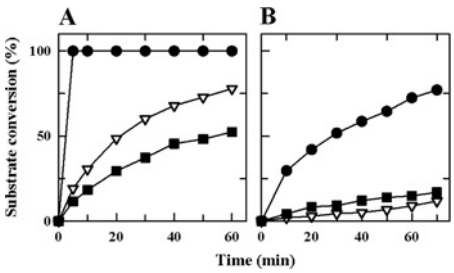

Figure 11 Time course of catalysis of GDP-*manno*-heptose and GDP-mannose by the T187V and T187N mutants of WcbK

Reactions of 24 μl containing 0.15 mM GDP-*manno*-heptose and 16 (**A**) or 5 (not shown) nmol of WcbK, or 0.15 mM GDP-mannose and 310 (**B**) or 155 (not shown) nmol of WcbK, were prepared in 200 mM Tris/HCl, pH 8.5, and incubated at 37 °C. At the indicated time points, 3 μl was withdrawn, flash-frozen at − 80 °C and analysed by CE extemporaneously after thawing and diluting one half in ice-cold water. The results are representative of the same trend observed in two independent experiments performed with two enzyme concentrations each. ●, Wild-type WcbK; ▽, T187N mutant; ■, T187V mutant.

Although increased catalysis of the GDP-mannose was anticipated in the T/N mutant compared with wild-type via restored coordination of the mannose C6 OH through the asparagine side chain, against expectations, this mutant only retained marginal ability to use GDP-mannose as a substrate relative to the wild-type (Figure 11B). Therefore, overall, these mutagenesis data identify Thr^{187} and its polar side chain as important for substrate binding and/or catalysis by WcbK, but point to the fact that other residues of the binding pocket may also contribute to substrate specificity by allowing a very precise fit of the substrate within the binding pocket. Our structural modelling has indicated quasi conservation of most residues involved in direct interactions with the substrate. Therefore other residues involved in shaping the binding pocket indirectly via their interactions with the conserved amino acids highlighted may also play a crucial role in substrate specificity.

DISCUSSION

The present study is the first biochemical analysis of two key enzymes of the 6-deoxy-*altro*-heptose biosynthesis pathway that is important for capsule synthesis in a variety of *Campylobacter* species. This work capitalized on our in-depth analyses of DmhA/DmhB, similar enzymes from the 6-deoxy-*manno*-heptose synthesis pathway in *Y. pseudotuberculosis*. Although the WcbK and WcaG enzymes were expected to have the basic C6 dehydratase and C4 reductase activities on the basis of global sequence similarities with DmhA/DmhB and on the basis of the presence of conserved catalytic residues, it was not known if WcbK/WcaG were also responsible for the sugar ring configuration change of the heptose from *manno* to *altro* or whether another enzyme was involved. Heptoses of altered configurations are present in the surface polysaccharides of a variety of *Campylobacter* species [13–15,25,41–44]. The corresponding gene clusters usually encode putative epimerase(s) that could be responsible for the ring configuration change(s) necessary in each strain [25,45], suggesting that the configuration of the heptose ring is retained during C6 dehydration. Our work on DmhA/DmhB demonstrated that this was the case in *Y. pseudotuberculosis* [23]. However, C6 dehydration can be accompanied by C5 epimerization [46], thereby resulting in inversion of the ring configuration. The presence of a putative C3,C5 epimerase reductase (Fcl) in the capsular cluster of *C. jejuni* 81-176 used for our present studies suggests that a C5 epimerization may occur concomitantly with the C6 dehydration step, and that the putative C3/C5 epimerase reductase may restore the original C5 configuration to produce the final 6-deoxy-*altro* compound. This would lead to the net result of a single C3 epimerization step. Therefore it was necessary to assess the situation for WcbK and WcaG.

The CE and MS analyses in the present study demonstrated the direct C6 dehydratase and C4 reductase activities for the enzymes, and also indicated that WcbK and WcaG can be substituted for their DmhA and DmhB homologues *in vitro*. This suggested that they can perform their reactions on the same substrates as DmhA and DmhB, and generate at least the same products as DmhA/DmhB. Final demonstration of lack of epimerization activity was obtained by NMR spectroscopy. Therefore the present study establishes that the reactions products of WcbK and WcaG are GDP-4-oxo-6-deoxy-*lyxo*-heptose and GDP-6-deoxy-*manno*-heptose respectively (Figures 1C and 1D).

However, the present study also revealed differences between the two enzyme pairs that may point to an alternative biosynthesis pathway of GDP-6-deoxy-*altro*-heptose in *C. jejuni* 81-176. First, an important difference between DmhA and WcbK was the greatly reduced catalytic activity of WcbK for GDP-*manno*-heptose compared with DmhA. Although this may at first sight indicate that GDP-*manno*-heptose is not the natural substrate for WcbK and that, *in vivo*, the C3 epimerization of the substrate may take place before C6 dehydration, the modelling data argue against this hypothesis. Conservation of the hydrogen bonding network for the sugar with that observed in the Mur1–GDP-rhamnose complex rather supports the notion that WcbK can only accommodate the *manno* configuration of the sugar. Therefore C3 epimerization probably occurs after the WcbK-mediated dehydration. Secondly, although it was not possible to determine kinetic parameters for WcaG for lack of stable substrate, semi-quantitative analyses performed using equimolar amounts of WcaG and DmhB enzymes indicated that catalysis was less efficient on the heptose-based substrate with WcaG than with DmhB (traces c on Figures 3B and 5A). In contrast, WcaG appeared more efficient at catalysing the mannose-based substrate than DmhB, although both enzymes had poor catalytic abilities with regards to this substrate. This also highlights the fact that the 4-oxo-6-deoxy-*lyxo*-heptose intermediate may not be the preferred substrate for WcaG and that C3 epimerization may occur before the WcaG-mediated reduction step *in vivo,* although after the activity of WcbK. Therefore the GDP-6-deoxy-*altro*-heptose synthesis pathway may be more complicated than anticipated, and its full elucidation will require the elucidation of the activity of the candidate epimerases present in the capsular cluster, such as Fcl (the potential C3,C5 epimerase mentioned above) and Cj1430 (a potential epimerase/reductase).

Examination of the substrate-binding sites of modelled enzymes showed that a conserved asparagine residue involved in coordination of the C6 OH of the hexose in GMD and Mur1 was replaced by a threonine in all heptose dehydratases (Thr^{187} in WcbK$_{CJ}$) and therefore appeared as a potential candidate determinant of substrate specificity. Although this residue was important for heptose catalysis, its mutations back to asparagine did not impart enhanced catalysis on GDP-mannose, and on the contrary decreased the ability of WcbK to use heptose as a substrate. Therefore additional residues are responsible for substrate specificity, and these would also be responsible for the differential catalytic abilities observed for DmhA and WcbK, both on heptose- and mannose-based substrates.

Finally, an interesting feature of WcbK and DmhA is their equal affinity for GDP-*manno*-heptose and GDP-mannose. The

K_m for both substrates are comparable with the K_m of known C6 dehydratases [47–49]. However, WcbK had higher catalytic efficiency than DmhA on GDP-mannose, suggesting that WcbK may have a dual activity *in vivo*: capsule synthesis via catalysis of GDP-*manno*-heptose, and an unknown function via catalysis of GDP-mannose. C6 dehydration of GDP-mannose is usually associated with the formation of GDP-rhamnose, GDP-L-fucose or GDP-perosamine [38,49,50], but neither rhamnose, fucose nor perosamine has been reported in the surface glycolipids of *C. jejuni*. As *C. jejuni* also produces a wide array of glycoproteins [51], it will be interesting in the future to investigate whether rhamnose, fucose or perosamine sugars are present on any glycoprotein, and if their presence is WcbK-dependent.

AUTHOR CONTRIBUTION

Carole Creuzenet performed half of the enzymology experiments, prepared some samples for MS, carried out the modelling studies, identified the residue to mutate, analysed all of the data, prepared all of the CE Figures, and wrote the paper. Matthew McCallum performed enzyme purifications, SDS/PAGE and Western blot analyses, performed WcbK kinetics, determined optimal activity parameters for WcbK and WcaG, made the WcbK mutants and tested their activity. He also made and purified reaction products for NMR spectroscopy and MS and prepared several of the Figures. Gary Shaw performed all NMR analyses and the associated data interpretation and Figure preparation, helped to finalize the modelling shown in Figure 9, performed the calculations for the accessible surface of the binding sites and edited the paper prior to submission.

ACKNOWLEDGEMENTS

We thank Nathan Ho and Tyler Kaster for cloning WcaG and WcbK in the pET vector, and Frank Butty for initial purifications of GDP-*manno*-heptose and WcaG. We thank Sari Kichler for initial assistance with protein purification. We thank Kathryn Barber for acquisition of the WcbK/WcaG NMR spectra.

FUNDING

This work was supported by operating grants from the Natural Sciences and Engineering Research Council (NSERC) of Canada [grant number RGPIN 240762-2010] (to C.C.)], and from the Canadian Institutes of Health Research [grant number MOP 93520] and the Canada Research Chairs programme (to G.S.). C.C. was the recipient of a University Faculty Award from NSERC.

REFERENCES

1 Lecuit, M., Abachin, E., Martin, A., Poyart, C., Pochart, P., Suarez, F., Bengoufa, D., Feuillard, J., Lavergne, A., Gordon, J. I. et al. (2004) Immunoproliferative small intestinal disease associated with *Campylobacter jejuni*. N. Engl. J. Med. **350**, 239–248
2 Lecuit, M. and Lortholary, O. (2005) Immunoproliferative small intestinal disease associated with *Campylobacter jejuni*. Med. Mal. Infect. **35**, S56–S58
3 Al-Saleem, T. and Al-Mondhiry, H. (2005) Immunoproliferative small intestinal disease (IPSID): a model for mature B-cell neoplasms. Blood **105**, 2274–2280
4 Zhao, S., Young, S. R., Tong, E., Abbott, J. W., Womack, N., Friedman, S. L. and McDermott, P. F. (2010) Antimicrobial resistance of *Campylobacter* isolates from retail meat in the United States between 2002 and 2007. Appl. Environ. Microbiol. **76**, 7949–7956
5 Sammarco, M. L., Ripabelli, G., Fanelli, I., Grasso, G. M. and Tamburro, M. (2010) Prevalence and biomolecular characterization of *Campylobacter* spp. isolated from retail meat. J. Food Prot. **73**, 720–728
6 Arsenault, J., Michel, P., Berke, O., Ravel, A. and Gosselin, P. (2011) Environmental characteristics associated with campylobacteriosis: accounting for the effect of age and season. Epidemiol. Infect., doi:10.1017/S0950268811000628
7 Alfredson, D. A. and Korolik, V. (2007) Antibiotic resistance and resistance mechanisms in *Campylobacter jejuni* and *Campylobacter coli*. FEMS Microbiol. Lett. **277**, 123–132
8 Larkin, C., Van Donkersgoed, C., Mahdi, A., Johnson, P., McNab, B. and Odumeru, J. (2006) Antibiotic resistance of *Campylobacter jejuni* and *Campylobacter coli* isolated from hog, beef, and chicken carcass samples from provincially inspected abattoirs in Ontario. J. Food Prot. **69**, 22–26
9 Cody, A. J., Clarke, L., Bowler, I. C. and Dingle, K. E. (2010) Ciprofloxacin-resistant campylobacteriosis in the UK. Lancet **376**, 1987
10 Bachtiar, B. M., Coloe, P. J. and Fry, B. N. (2007) Knockout mutagenesis of the *kpsE* gene of *Campylobacter jejuni* 81116 and its involvement in bacterium–host interactions. FEMS Immunol. Med. Microbiol. **49**, 149–154
11 Bacon, D. J., Szymanski, C. M., Burr, D. H., Silver, R. P., Alm, R. A. and Guerry, P. (2001) A phase-variable capsule is involved in virulence of *Campylobacter jejuni* 81-176. Mol. Microbiol. **40**, 769–777
12 Jones, M. A., Marston, K. L., Woodall, C. A., Maskell, D. J., Linton, D., Karlyshev, A. V., Dorrell, N., Wren, B. W. and Barrow, P. A. (2004) Adaptation of *Campylobacter jejuni* NCTC11168 to high-level colonization of the avian gastrointestinal tract. Infect. Immun. **72**, 3769–3776
13 Aspinall, G. O., McDonald, A. G. and Pang, H. (1992) Structures of the O chains from lipopolysaccharides of *Campylobacter jejuni* serotypes O:23 and O:36. Carbohydr. Res. **231**, 13–30
14 Chen, Y. H., Poly, F., Pakulski, Z., Guerry, P. and Monteiro, M. A. (2008) The chemical structure and genetic locus of *Campylobacter jejuni* CG8486 (serotype HS:4) capsular polysaccharide: the identification of 6-deoxy-D-*ido*-heptopyranose. Carbohydr. Res. **343**, 1034–1040
15 St Michael, F., Szymanski, C. M., Li, J., Chan, K. H., Khieu, N. H., Larocque, S., Wakarchuk, W. W., Brisson, J. R. and Monteiro, M. A. (2002) The structures of the lipooligosaccharide and capsule polysaccharide of *Campylobacter jejuni* genome sequenced strain NCTC 11168. Eur. J. Biochem. **269**, 5119–5136
16 Aspinall, G. O., Lynch, C. M., Pang, H., Shaver, R. T. and Moran, A. P. (1995) Chemical structures of the core region of *Campylobacter jejuni* O:3 lipopolysaccharide and an associated polysaccharide. Eur. J. Biochem. **231**, 570–578
17 Reckseidler, S. L., DeShazer, D., Sokol, P. A. and Woods, D. E. (2001) Detection of bacterial virulence genes by subtractive hybridization: identification of capsular polysaccharide of *Burkholderia pseudomallei* as a major virulence determinant. Infect. Immun. **69**, 34–44
18 Reckseidler-Zenteno, S. L., DeVinney, R. and Woods, D. E. (2005) The capsular polysaccharide of *Burkholderia pseudomallei* contributes to survival in serum by reducing complement factor C3b deposition. Infect. Immun. **73**, 1106–1115
19 Samuelsson, K., Lindberg, B. and Brubaker, R. R. (1974) Structure of O-specific side chains of lipopolysaccharides from *Yersinia pseudotuberculosis*. J. Bacteriol. **117**, 1010–1016
20 Komandrova, N. A., Gorshkova, R. P., Isakov, V. V. and Ovodov, Iu S. (1984) Structure of O-specific polysaccharide isolated from the *Yersinia pseudotuberculosis* serotype 1A lipopolysaccharide. Bioorg. Khim. **10**, 232–237
21 Skurnik, M. and Zhang, L. (1996) Molecular genetics and biochemistry of *Yersinia* lipopolysaccharide. APMIS **104**, 849–872
22 Ho, N., Kondakova, A. N., Knirel, Y. A. and Creuzenet, C. (2008) The biosynthesis and biological role of 6-deoxyheptose in the lipopolysaccharide O-antigen of *Yersinia pseudotuberculosis*. Mol. Microbiol. **68**, 424–447
23 Butty, F. D., Aucoin, M., Morrison, L., Ho, N., Shaw, G. and Creuzenet, C. (2009) Elucidating the formation of 6-deoxyheptose: biochemical characterization of the GDP-D-glycero-D-*manno*-heptose C6 dehydratase, DmhA and its associated C4 reductase DmhB. Biochemistry **48**, 7764–7775
24 Kondakova, A. N., Ho, N., Bystrova, O. V., Shashkov, A. S., Lindner, B., Creuzenet, C. and Knirel, Y. A. (2008) Structural studies of the O-antigens of *Yersinia pseudotuberculosis* O:2a and mutants thereof with impaired 6-deoxy-D-manno-heptose biosynthesis pathway. Carbohydr. Res. **343**, 1383–1389
25 Karlyshev, A. V., Champion, O. L., Churcher, C., Brisson, J. R., Jarrell, H. C., Gilbert, M., Brochu, D., St Michael, F., Li, J., Wakarchuk, W. W. et al. (2005) Analysis of *Campylobacter jejuni* capsular loci reveals multiple mechanisms for the generation of structural diversity and the ability to form complex heptoses. Mol. Microbiol. **55**, 90–103
26 Newton, D. T. and Mangroo, D. (1999) Mapping the active site of the *Haemophilus influenzae* methionyl-tRNA formyltransferase: residues important for catalysis and tRNA binding. Biochem. J. **339**, 63–69
27 Demendi, M., Ishiyama, N., Lam, J. S., Berghuis, A. M. and Creuzenet, C. (2005) Towards a better understanding of the substrate specificity of the UDP-*N*-acetylglucosamine C4 epimerase WbpP. Biochem. J. **389**, 173–180
28 Obhi, R. K. and Creuzenet, C. (2005) Biochemical characterization of the *Campylobacter jejuni* Cj1294, a novel UDP-4-keto-6-deoxy-GlcNAc aminotransferase that generates UDP-4-amino-4,6-dideoxy-GalNAc. J. Biol. Chem. **280**, 20902–20908
29 Bax, A. and Davis, D. G. (1985) MLEV-17-Based two-dimensional homonuclear magnetization transfer spectroscopy. J. Magn. Reson. **65**, 355–360
30 Kay, L. E., Keifer, P. and Saarinen, T. (1992) Pure absorption gradient enhanced heteronuclear single quantum correlation spectroscopy with improved sensitivity. J. Am. Chem. Soc. **114**, 10663–10665

31 John, B. K., Plant, D. and Hurd, R. E. (1992) Improved proton-detected heteronuclear correlation using gradient-enhanced z and zz filters. J. Magn. Reson. **A101**, 113–117
32 Webb, N. A., Mulichak, A. M., Lam, J. S., Rocchetta, H. L. and Garavito, R. M. (2004) Crystal structure of a tetrameric GDP-D-mannose 4,6-dehydratase from a bacterial GDP-D-rhamnose biosynthetic pathway. Protein Sci. **13**, 529–539
33 Mulichak, A. M., Bonin, C. P., Reiter, W. D. and Garavito, R. M. (2002) Structure of the MUR1 GDP-mannose 4,6-dehydratase from *Arabidopsis thaliana:* implications for ligand binding and specificity. Biochemistry **41**, 15578–15589
34 Sobolev, V., Sorokine, A., Prilusky, J., Abola, E. E. and Edelman, M. (1999) Automated analysis of interatomic contacts in proteins. Bioinformatics **15**, 327–332
35 Willard, L., Ranjan, A., Zhang, H., Monzavi, H., Boyko, R. F., Sykes, B. D. and Wishart, D. S. (2003) VADAR: a web server for quantitative evaluation of protein structure quality. Nucleic Acids Res. **31**, 3316–3319
36 Somoza, J. R., Menon, S., Schmidt, H., Joseph-McCarthy, D., Dessen, A., Stahl, M. L., Somers, W. S. and Sullivan, F. X. (2000) Structural and kinetic analysis of *Escherichia coli* GDP-mannose 4,6 dehydratase provides insights into the enzyme's catalytic mechanism and regulation by GDP-fucose. Structure **8**, 123–135
37 Zhao, G., Liu, J., Liu, X., Chen, M., Zhang, H. and Wang, P. G. (2007) Cloning and characterization of GDP-perosamine synthetase (Per) from *Escherichia coli* O157:H7 and synthesis of GDP-perosamine *in vitro*. Biochem. Biophys. Res. Commun. **363**, 525–530
38 King, J. D., Poon, K. K., Webb, N. A., Anderson, E. M., McNally, D. J., Brisson, J. R., Messner, P., Garavito, R. M. and Lam, J. S. (2009) The structural basis for catalytic function of GMD and RMD, two closely related enzymes from the GDP-D-rhamnose biosynthesis pathway. FEBS J. **276**, 2686–700
39 Maki, M., Jarvinen, N., Rabina, J., Roos, C., Maaheimo, H. and Renkonen, R. (2002) Functional expression of *Pseudomonas aeruginosa* GDP-4-keto-6-deoxy-D-mannose reductase which synthesizes GDP-rhamnose. Eur. J. Biochem. **269**, 593–601
40 Kneidinger, B., Graninger, M., Adam, G., Puchberger, M., Kosma, P., Zayni, S. and Messner, P. (2001) Identification of two GDP-6-deoxy-D-lyxo-4-hexulose reductases synthesizing GDP-D-rhamnose in *Aneurinibacillus thermoaerophilus* L420–91T. J. Biol. Chem. **276**, 5577–5583
41 Aspinall, G. O., McDonald, A. G., Pang, H., Kurjanczyk, L. A. and Penner, J. L. (1993) An antigenic polysaccharide from *Campylobacter coli* serotype O:30. Structure of a teichoic acid-like antigenic polysaccharide associated with the lipopolysaccharide. J. Biol. Chem. **268**, 18321–18329
42 Aspinall, G. O., McDonald, A. G., Pang, H., Kurjanczyk, L. A. and Penner, J. L. (1993) Lipopolysaccharide of *Campylobacter coli* serotype O:30. Fractionation and structure of liberated core oligosaccharide. J. Biol. Chem. **268**, 6263–6268
43 Aspinall, G. O., Monteiro, M. A. and Pang, H. (1995) Lipo-oligosaccharide of the *Campylobacter lari* type strain ATCC 35221. Structure of the liberated oligosaccharide and an associated extracellular polysaccharide. Carbohydr. Res. **279**, 245–264
44 Hanniffy, O. M., Shashkov, A. S., Moran, A. P., Prendergast, M. M., Senchenkova, S. N., Knirel, Y. A. and Savage, A. V. (1999) Chemical structure of a polysaccharide from *Campylobacter jejuni* 176.83 (serotype O:41) containing only furanose sugars. Carbohydr. Res. **319**, 124–132
45 Parkhill, J., Wren, B. W., Mungall, K., Ketley, J. M., Churcher, C., Basham, D., Chillingworth, T., Davies, R. M., Feltwell, T., Holroyd, S. et al. (2000) The genome sequence of the food-borne pathogen *Campylobacter jejuni* reveals hypervariable sequences. Nature **403**, 665–668
46 Schoenhofen, I. C., McNally, D. J., Vinogradov, E., Whitfield, D., Young, N. M., Dick, S., Wakarchuk, W. W., Brisson, J. R. and Logan, S. M. (2006) Functional characterization of dehydratase/aminotransferase pairs from *Helicobacter* and *Campylobacter*: enzymes distinguishing the pseudaminic acid and bacillosamine biosynthetic pathways. J. Biol. Chem. **281**, 723–732
47 Sullivan, F. X., Kumar, R., Kriz, R., Stahl, M., Xu, G. Y., Rouse, J., Chang, X. J., Boodhoo, A., Potvin, B. and Cumming, D. A. (1998) Molecular cloning of human GDP-mannose 4,6-dehydratase and reconstitution of GDP-fucose biosynthesis *in vitro*. J. Biol. Chem. **273**, 8193–8202
48 Sturla, L., Bisso, A., Zanardi, D., Benatti, U., De Flora, A. and Tonetti, M. (1997) Expression, purification and characterization of GDP-D-mannose 4,6-dehydratase from *Escherichia coli*. FEBS Lett. **412**, 126–130
49 Wu, B., Zhang, Y. and Wang, P. G. (2001) Identification and characterization of GDP-D-mannose 4,6-dehydratase and GDP-L-fucose synthetase in a GDP-L-fucose biosynthetic gene cluster from *Helicobacter pylori*. Biochem. Biophys. Res. Commun. **285**, 364–371
50 Albermann, C. and Piepersberg, W. (2001) Expression and identification of the RfbE protein from *Vibrio cholerae* O1 and its use for the enzymatic synthesis of GDP-D-perosamine. Glycobiology **11**, 655–661
51 Szymanski, C. M., Yao, R., Ewing, C. P., Trust, T. J. and Guerry, P. (1999) Evidence for a system of general protein glycosylation in *Campylobacter jejuni*. Mol. Microbiol. **32**, 1022–1030

Received 19 May 2011/21 June 2011; accepted 28 June 2011
Published as BJ Immediate Publication 28 June 2011, doi:10.1042/BJ20110890

Biochem. J. (2011) **439**, 235–248 (Printed in Great Britain) doi:10.1042/BJ20110890

online data

SUPPLEMENTARY ONLINE DATA

Characterization of the dehydratase WcbK and the reductase WcaG involved in GDP-6-deoxy-*manno*-heptose biosynthesis in *Campylobacter jejuni*

Matthew McCALLUM*, Gary S. SHAW† and Carole CREUZENET*[1]

*Department of Microbiology and Immunology, Infectious Diseases Research Group, University of Western Ontario, London, ON, Canada, N6A 5C1, and †Department of Biochemistry, University of Western Ontario, London, ON, Canada, N6A 5C1

Supplementary Figure S1 is available on the following page.

[1] To whom correspondence should be addressed (email ccreuzen@uwo.ca).

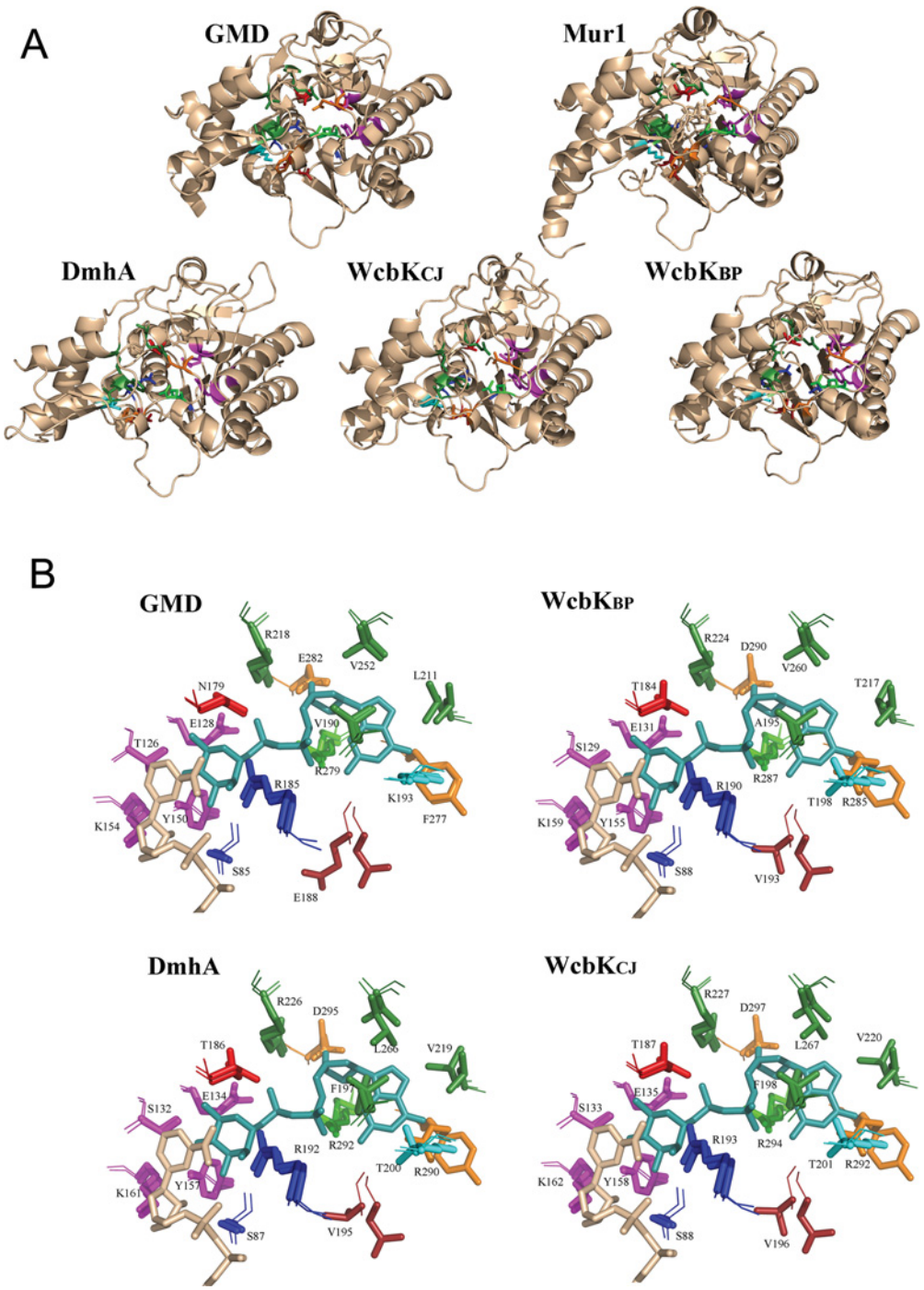

Figure S1 Structural modelling of GDP-*manno*-heptose dehydratases

The models for the *C. jejuni* 81-176 WcbK ($WcbK_{CJ}$) and its homologues from *B. pseudomallei* ($WcbK_{BP}$) and *Y. pseudotuberculosis* (DmhA) were created using SwissModel and visualized with PyMol. (**A**) The structures of the three GDP-*manno*-heptose dehydratases are shown, along with the structures of the GDP-mannose dehydratases GMD (from *P. aeruginosa*) and Mur1 (from *A. thaliana*) that were used to model them. The view of all of the proteins is through the Rossmann fold. The cofactor and reaction product GDP-rhamnose that were co-crystallized with Mur1 are shown in the Mur1 structure. (**B**) Zoomed-in active sites overlaid with the active site of Mur1 that comprised its cofactor (beige sticks) and GDP-rhamnose (light blue sticks). The numbered amino acid residues correspond to each structure displayed (not to the Mur1 template used for alignment). In (**A**) and (**B**), residues important for substrate and cofactor binding and catalysis are highlighted in colour. The conserved catalytic serine/threonine, glutamic acid, tyrosine and lysine residues are in magenta. Residues involved in sugar binding and conserved in all proteins are in dark blue. Residues involved in GDP binding and conserved in all proteins are in green. All other coloured residues are different in the mannose dehydratases compared with the *manno*-heptose dehydratases, but are conserved within each category. See the main text for details.

Received 19 May 2011/21 June 2011; accepted 28 June 2011
Published as BJ Immediate Publication 28 June 2011, doi:10.1042/BJ20110890